DISCLAIMERS

DISPOSITION INSTRUCTIONS

ii

SUMMARY

An investigation has been performed to analytically determine the flow field about a helicopter fuselage and to apply the results to the prediction of parasite drag. The analytical method is currently restricted to nonlifting bodies in nonyawed flow. The flow field is determined by using the Douglas-Neumann computer program for the potential field and a boundary layer analysis based upon the small cross-flow assumption. Pressure distribution correlation between test data and the Douglas-Neumann program is very good except for areas of separated flow. Agreement is also good between boundary layer velocity profiles obtained from test data and from the boundary layer analysis. An empirical approach based on test data is used to approximate the pressure in the separated region. Drag is obtained by numerical integration of the pressure and skin friction distribution. Agreement is reasonable between test data and the drag obtained by the summation process. The analytical method has potential application in the design of helicopter fuselages of minimum parasite drag.

AD-777798

DOCUMENT CONTROL DATA - R & D

(Security classification of title, body of abstract and indexing annotation must be entered when the overall report is classified)

1. ORIGINATING ACTIVITY (Corporate author)	2a. REPORT SECURITY CLASSIFICATION
Eustis Directorate U.S. Army Air Mobility Research and Development Laboratory Fort Eustis, Virginia	Unclassified
	2b. GROUP

3. REPORT TITLE

AN EXPERIMENTAL AND ANALYTICAL INVESTIGATION OF THE POTENTIAL FLOW FIELD, BOUNDARY LAYER, AND DRAG OF VARIOUS HELICOPTER FUSELAGE CONFIGURATIONS

4. DESCRIPTIVE NOTES (Type of report and inclusive dates)

5. AUTHOR(S) (First name, middle initial, last name)

James Gillespie, Jr.
Richard I. Windsor

6. REPORT DATE	7a. TOTAL NO. OF PAGES	7b. NO. OF REFS
January 1974	62	5

8a. CONTRACT OR GRANT NO.	9a. ORIGINATOR'S REPORT NUMBER(S)
b. PROJECT NO.	USAAMRDL Technical Note 13
c. House Task 72-09	9b. OTHER REPORT NO(S) (Any other numbers that may be assigned this report)
d.	

10. DISTRIBUTION STATEMENT

Approved for public release; distribution unlimited.

11. SUPPLEMENTARY NOTES	12. SPONSORING MILITARY ACTIVITY
	Eustis Directorate, U. S. Army Air Mobility Research and Development Laboratory Fort Eustis, Virginia

13. ABSTRACT

An investigation has been performed to analytically determine the flow field about a helicopter fuselage and to apply the results to the prediction of parasite drag. The analytical method is currently restricted to nonlifting bodies in nonyawed flow. The flow field is determined by using the Douglas-Neumann computer program for the potential field and a boundary layer analysis based upon the small cross-flow assumption. Pressure distribution correlation between test data and the Douglas-Neumann program is very good except for areas of separated flow. Agreement is also good between boundary layer velocity profiles obtained from test data and from the boundary layer analysis. An empirical approach based on test data is used to approximate the pressure in the separated region. Drag is obtained by numerical integration of the pressure and skin friction distribution. Agreement is reasonable between test data and the drag obtained by the summation process. The analytical method has potential application in the design of helicopter fuselages of minimum parasite drag.

DD FORM 1473, 1 NOV 65

REPLACES DO FORM 1473, 1 JAN 64, WHICH IS OBSOLETE FOR ARMY USE.

14. KEY WORDS	LINK A		LINK B		LINK C	
	ROLE	WT	ROLE	WT	ROLE	WT
Fuselage Drag						
Potential Flow						
Boundary Layer						

FOREWORD

v

TABLE OF CONTENTS

Preceding page blank

LIST OF ILLUSTRATIONS

LIST OF TABLES

LIST OF SYMBOLS

C_p	pressure coefficient
D	drag, lb
M_∞	free-stream Mach number
q	dynamic pressure, lb/sq ft
u	local velocity, mph
U	local velocity at edge of boundary layer, mph
V_∞	free-stream velocity, mph
Y	height above model surface, in.
a	angle of attack, deg
δ	boundary layer thickness, in.
ψ	sideslip angle, deg

INTRODUCTION

Helicopter fuselage aerodynamics has been generally neglected as compared to rotor aero-
dynamics. As a result, there has been a great reliance on wind tunnel testing to produce
fuselage aerodynamic data for helicopter performance and dynamic analyses. Generally,
extensive drag buildup wind tunnel tests are performed on fuselage scale models without
rotors to obtain fuselage parasite drag. Drag estimates are generally based on handbook-
type methods such as those discussed by Hoerner.[1] There is a need to develop more
advanced analytical procedures to determine the fuselage flow field and drag, thereby
reducing the amount of wind tunnel test time presently required and resulting in more
efficient fuselage designs. Advanced analytical procedures would be especially useful in
the design of advanced high-speed helicopters. At high forward speed, parasite drag becomes
increasingly important in helicopter performance. The horsepower required to overcome
parasite drag is proportional to the cube of the forward velocity. Thus, a high-speed heli-
copter fuselage should be aerodynamically clean. The reduction of areas of flow separation
will result in fuselages of lower parasite drag. An advanced flow-field analysis could identify
areas of separated flow and allow for the investigation of alternate configurations to mini-
mize separation. Reliable pressure data, also useful to the structural designer, could be
easily obtained from a flow-field analysis.

The solution of three-dimensional flow existing around a body such as a helicopter
fuselage is a formidable problem. However, numerous potential flow and boundary layer
methods have been recently developed. The basic assumptions used in the flow-field
analysis are arbitrary body, nonlifting body, and small cross flow in the boundary layer.
Three computer programs used in this flow-field analysis are:

- Douglas-Neumann potential flow computer program.[2]

- A streamline computer program.[3]

- A boundary layer computer program.[4]

In order to verify analytical procedures, suitable data must exist to provide correlation
between test and theory and to aid in understanding the actual fluid physics. The
University of Maryland, under an Army contract, conducted the experimental investigation
and provided the test data. This investigation was performed in the University of Mary-
land 8- by 11-foot wind tunnel and provided detailed pressure measurements, boundary
layer velocity profiles, flow visualization, and overall forces and moments on various
helicopter fuselage configurations. Limited pressure data were also available from tests
conducted at NASA-Langley and Sikorsky.

This report describes the use of the computer programs, giving program limitations and
computer times. Data generated by the computer programs and wind tunnel tests are
compared. The procedure for using the computer programs to determine parasite drag is
described. The procedure is incomplete in that a method for predicting pressure distribu-
tions due to flow separation must be developed. By using test data, it is shown that
reasonable fuselage drag prediction could be made if pressure distributions due to flow
separation could be determined.

1

DOUGLAS-NEUMANN POTENTIAL FLOW PROGRAM

The Douglas-Neumann program is discussed in Reference 2. The fully three-dimensional nonlifting version of the program was used in the analysis. The fuselage body is approximated by a series of plane quadrilateral panels. Each panel represents a source that simulates the potential flow field of the body. The accuracy of the solution increases with an increasing number of panels, as does the computer time required. Thus, a compromise between the desired accuracy and computer time is required. Approximately 250 to 350 source panels are used in this analysis. Central Processing Unit time on a CDC-6600 is about 5 minutes per case. For a basic geometric configuration, different angles of attack and yaw angles may be run at only a slight increase in computer time.

The program determines the pressure coefficient (C_p) at a reference point on each source panel and at any specified off-body point. However, the location of the reference point on the panel is not known beforehand. This usually means that data must be interpolated to provide correlation at similar points for the program and experiment. In the University of Maryland tests the pressure orifices were located to generally coincide with the reference points in the computer program, thus minimizing interpolation and extrapolation.

The program has no body shape limitations in the subsonic flow field. Results were obtained in all cases for incompressible flow, even though compressibility correction options are available. Input data to the program consists of a series of geometric points that describe the body. Input is somewhat of an art, since the user must determine the size and number of panels. Panels are determined by four input corner points. However, three points are sufficient to determine a plane panel, and the program adjusts the points so that they lie in a plane. Thus, in regions of high curvature the panel size must be smaller so that the plane panel is a better approximation of the body. Each panel must be carefully checked to see that it closely approximates the actual body.

In order to become familiar with the computer program and provide some correlation with test data, the fuselage model used in Reference 5 was analyzed. Pressure orifices were located only on the pylon, as shown in Figure 1. The theoretical results and test data of Reference 5 are compared in Figures 2 and 3. Nondimensional pressure coefficient (C_p) is plotted versus axial distance on the pylon for a free-stream Mach number of 0.2. Agreement is quite good for the 30-degree and 150-degree pressure tap data shown in Figure 2. Agreement is not so good for the 60-degree and 120-degree pressure tap data shown in Figure 3. This area is more difficult to model accurately, and some flow separation may be occurring after the +4 axial station where a steep adverse pressure gradient exists. The comparison provided experience in the use of the program and a degree of confidence in the results of the program.
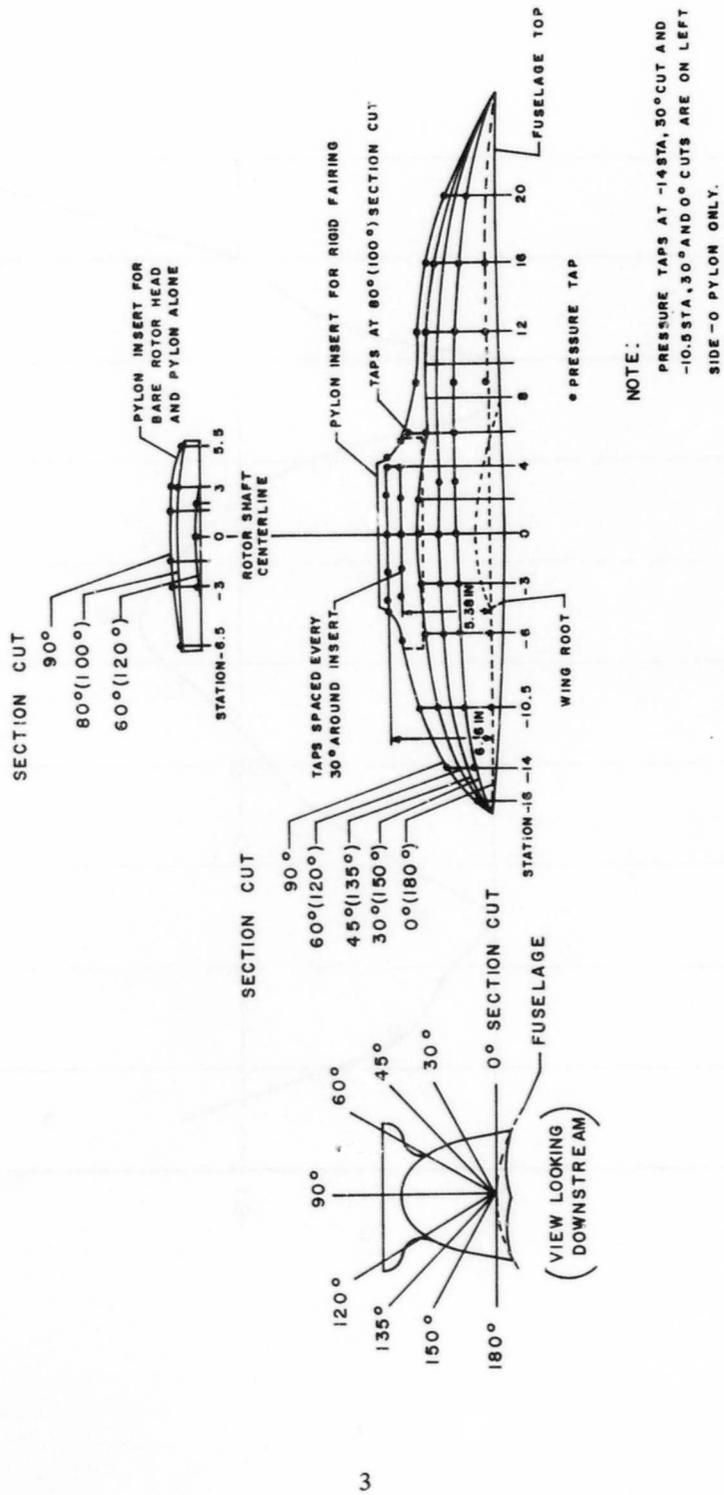
Figure 1. Pylon Used in Sikorsky Test Program.

3
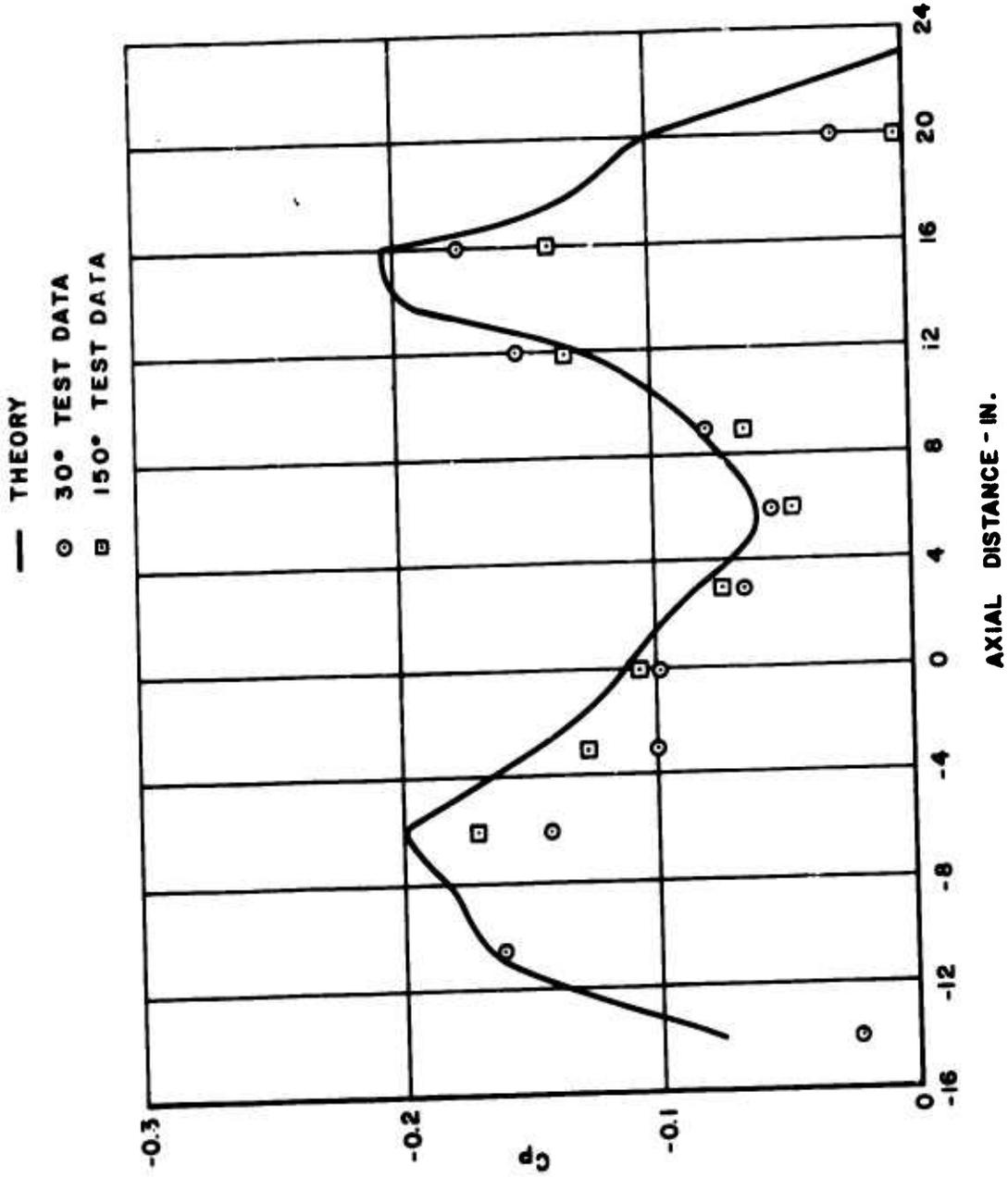
Figure 2. Pressure Coefficient Versus Axial Distance; $M_\infty = 0.2$, $\alpha = 0$ Deg.

4
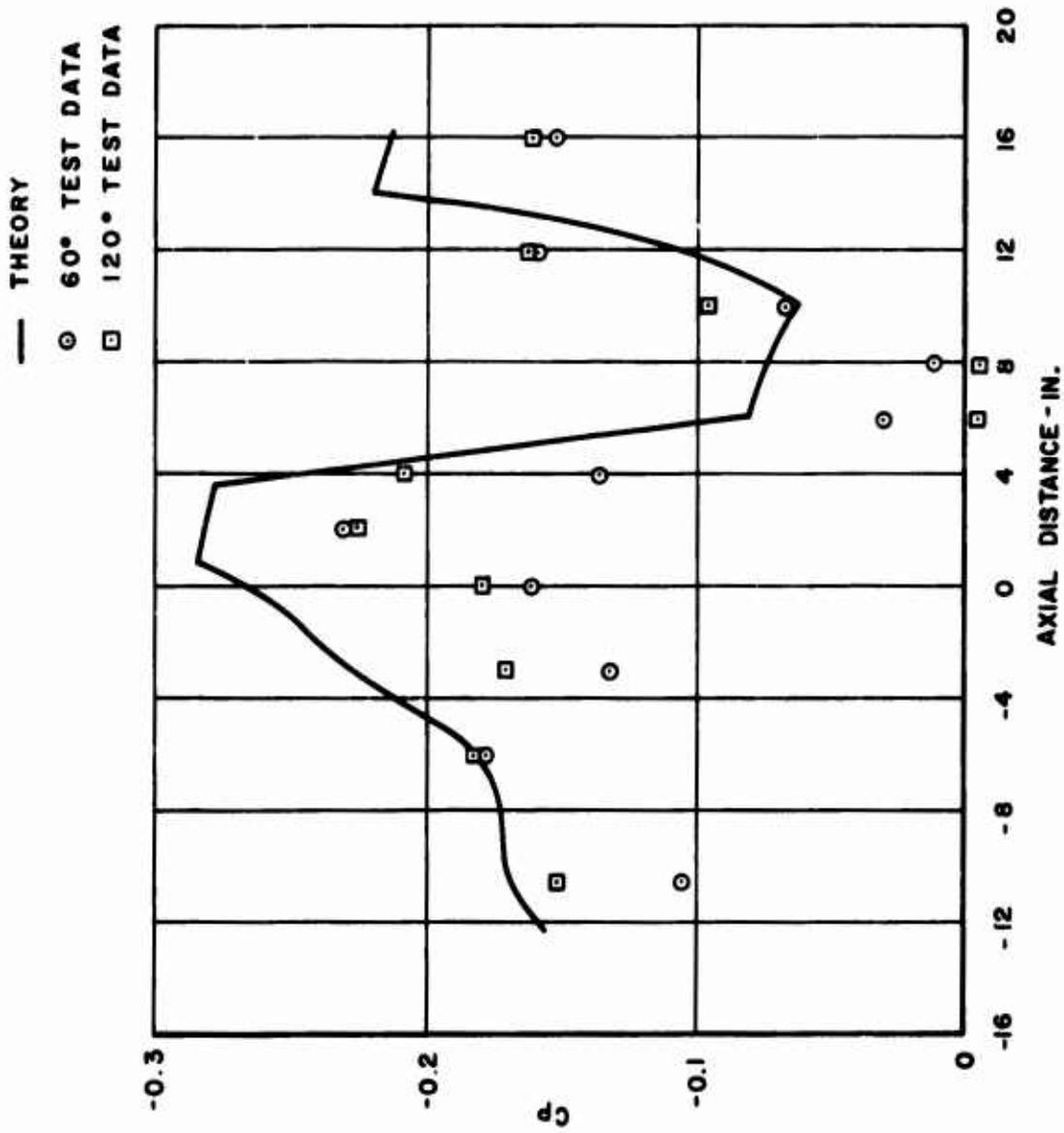
Figure 3. Pressure Coefficient Versus Axial Distance; $M_\infty = 0.2$, $\alpha = 0$ Deg.

5

BOUNDARY LAYER ANALYSIS

Fully three-dimensional boundary layer computer programs are not readily available; therefore, the small cross-flow assumption has been used to account for three-dimensional effects. This method was suggested by Dr. J. E Harris, NASA-Langley, who developed the boundary layer computer program used in the analysis. An axisymmetric boundary layer is calculated along streamlines with the radius replaced by the streamline divergence. A separate computer program is used to compute streamlines and the streamline divergence.

The streamline computer program described in Reference 3 is restricted to flows having the free-stream velocity vector in a plane of symmetry. Therefore, streamlines of yawed fuselages cannot be determined using this computer program. A further restriction is imposed by the use of spline functions to curve-fit the body. The coordinate system origin is at the nose of the body, and each body cross section must contain the coordinate system. The streamlines can only be determined up to the point where the body cross sections contain the coordinate system, as was the case in one of the configurations used in this analysis. However, flow separation occurs on the body ahead of this point. Since the boundary layer analysis is valid only up to flow separation, no difficulty is encountered.

Input to the streamline computer program consists of geometric points describing the body and free-stream conditions. Streamlines may be calculated from a specified inviscid pressure distribution, from a modified Newtonian pressure distribution, or from the body geometry alone. Numerical difficulties were encountered in the use of pressure distributions from the Douglas-Neumann program. For the low subsonic speed regime, the ratio of static pressure to stagnation pressure is very nearly 1.0 over all the body. This quantity is differentiated along a streamline, and the numerical results were unstable. Because of this, the simplified method based solely on body geometry was used. Running time is approximately 2 minutes for seven streamlines on the CDC-6600.

The boundary layer computer program described in Reference 4 solves the compressible laminar, transitional, or turbulent boundary layer equations for planar or axisymmetric flows. In the present analysis the axisymmetric version was used along streamlines with the body radius replaced by the streamline divergence. The input to the program consists of tables of axial distance, streamline distance, inviscid pressure distribution, and stream-line divergence. Running times are approximately 4 minutes per streamline on the CDC-6600. One fuselage configuration investigated required about seven streamlines to determine the skin friction distribution over the body for one test condition. The program was used to determine areas of flow separation on the body using vanishing skin friction as the criterion for flow separation.

LANGLEY TEST PROGRAM

In order to become familiar with the streamline and boundary layer computer programs, a model helicopter fuselage that had been tested in the NASA-Langley wind tunnel was analyzed (see Figure 4). Pressure tap orifice locations are shown in the figure. The potential flow field was determined by using the Douglas-Neumann computer program. Test data and the analytic predictions are compared in Figure 5, which gives pressure coefficient versus axial distance on different parts of the body for a free-stream velocity of 60 knots. Results are for zero yaw and angle of attack. Agreement is quite good except in regions of separation on the bottom and top of the body. There are some regions of severe adverse pressure gradients well forward on the body, and there is probably some local flow separation.

Seven streamlines were located on the body by using the streamline computer program. This program determined the streamline divergence as a function of streamline distance. The bottom streamline was chosen for a boundary layer analysis using the inviscid pressure distribution shown for the bottom centerline case. The boundary layer program indicated flow separation at an axial station of 2 inches where a steep adverse pressure gradient is encountered. The program predicted separation even when the pressure distribution was changed to the actual test data. Unfortunately, no separation studies were performed during the wind tunnel tests. It was necessary to select body shapes with less steep adverse pressure gradients on the forward portion of the body in order to become knowledgeable in the use of the boundary layer program.

• DENOTES LOCATION CF PRESSURE TAP
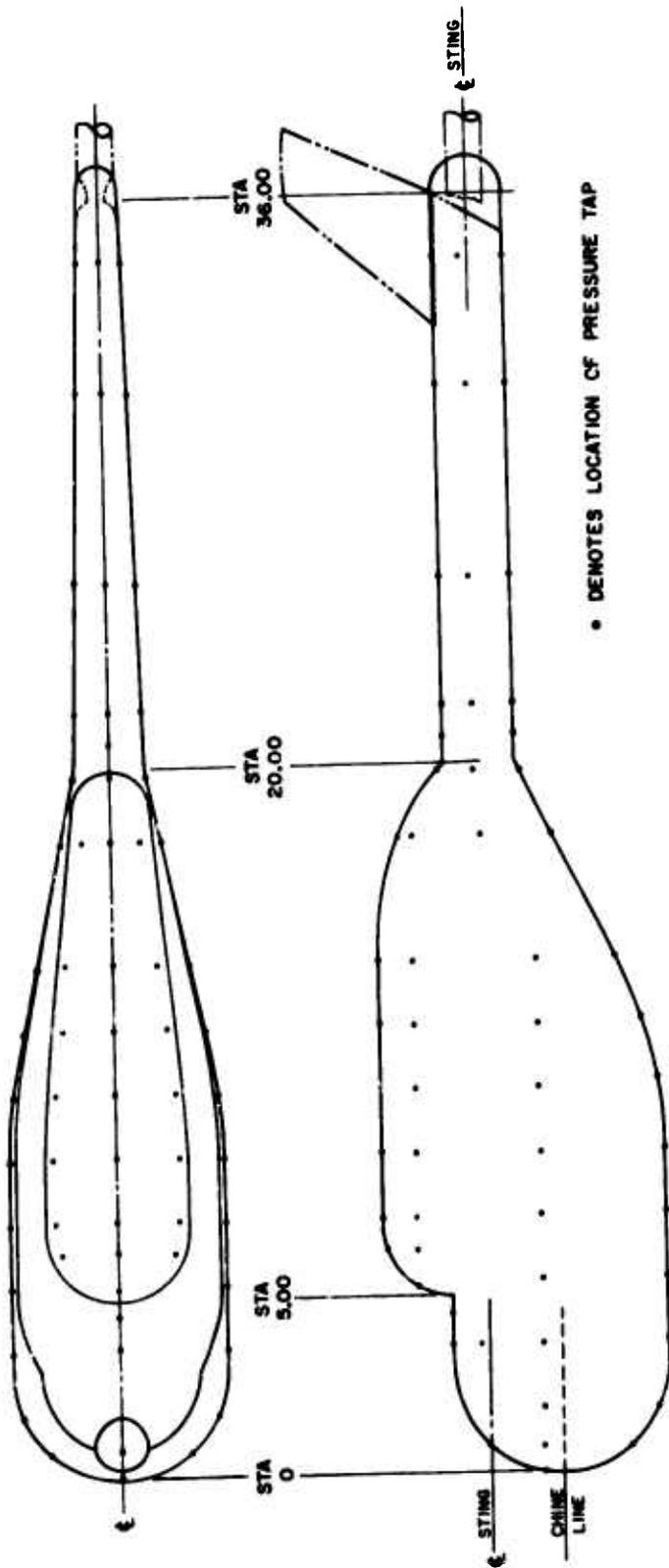
Figure 4. Model Used in Langley Test Program.

8
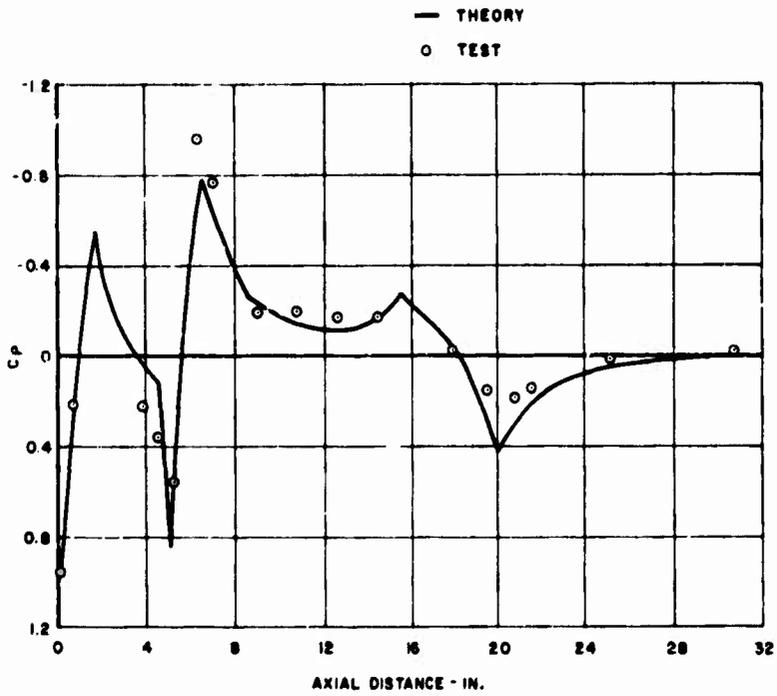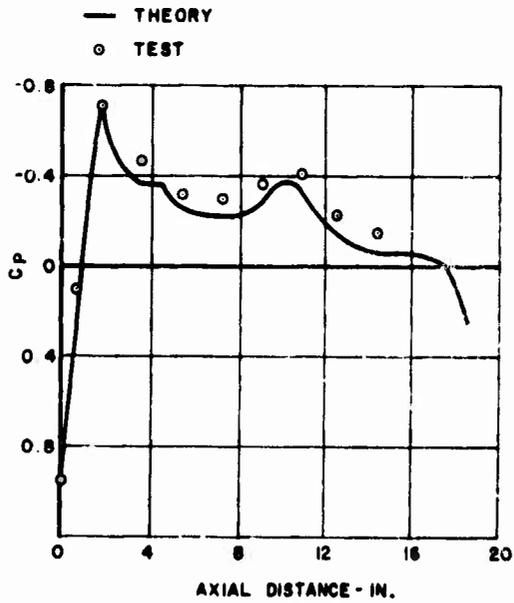
Top Centerline

Midfuselage

Figure 5. Pressure Coefficient Versus Axial Distance;
$V_\infty = 60$ Kt, $a = 0$ Deg.

9
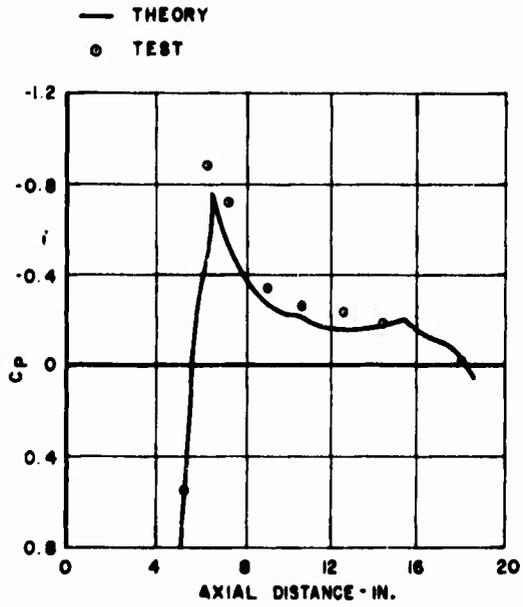
Side of Pylon
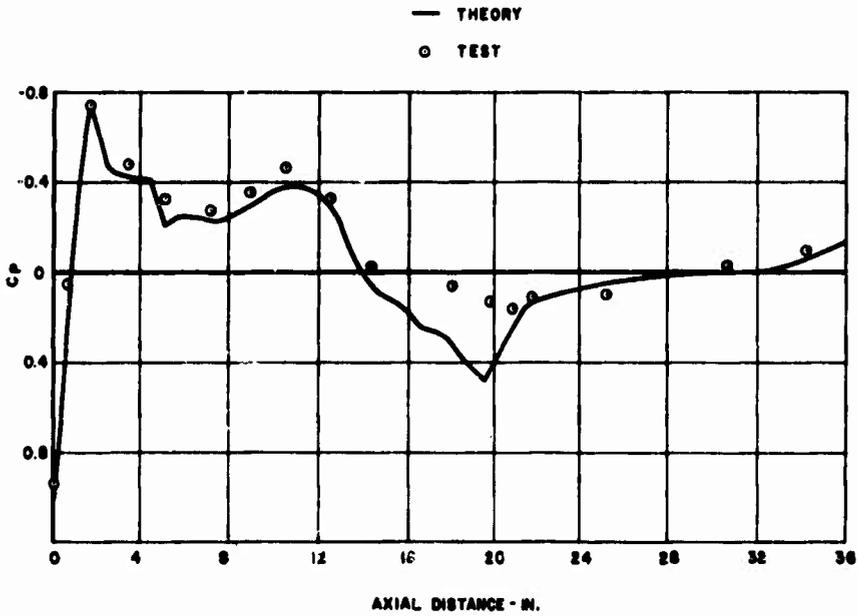
Bottom Centerline

Figure 5. Concluded.

COMPARISON OF TEST DATA AND ANALYSIS

GENERAL DISCUSSION

A ¼-scale fiberglass model of the BO-105 was selected for the wind tunnel test program at the University of Maryland (see Figure 6). Horizontal and vertical tail surfaces were removed to simplify the analytical model. Since the pylon can be removed from the model, tests were conducted on configurations with and without the pylon. Tests were also conducted on pylon-skid and pylon-skid/rotor hub configurations. In addition, an alternate nose configuration was designed to investigate its effect on the flow field. The alternate nose configuration is shown by the dashed lines in Figure 6.

The coordinate system used in the analysis is shown in Figure 6. Waterline 6 coincides with the X-axis, the axis from which the angle of attack is measured. Locations of other waterlines, key fuselage stations, and the boundary layer probe are also shown. Up to 265 pressure taps, located along the top centerline, bottom centerline, and various waterlines, were used in the test program.

Tests were conducted at free-stream velocities of 100, 150, and 200 mph. Most of the tests were at 150 mph. Angle of attack was varied from +15 to −15 degrees in 5-degree increments. Yaw angle was also varied from +15 degrees to −15 degrees in 5-degree increments. Since the streamline analysis is valid only for nonyawed flow, all comparisons of test data and theory are for the zero yaw condition.

The test program generated a great deal of data above that required to verify the analytic method. A complete set of tabulated test data is available from the Eustis Directorate. The test program is described in the appendix.

PRESSURE DISTRIBUTION

Approximately 300 source panels were used in the potential flow model for the fuselage without pylon. Test data and theory are compared in Figure 7 for cases representing the zero-angle-of-attack and the extreme-angle-of-attack ranges of the test program. Pressure distributions have been plotted versus axial distance along the top and bottom centerlines and along waterline 6. Agreement between test and theory is very good except in the flow-separated region at the aft end of the main fuselage. Flow separation is caused by a strong adverse pressure gradient in this region.

About 50 more source panels were added to the basic fuselage model to represent the pylon. The test data and theory are compared in Figure 8 for representative cases. The flow approaches stagnation in front of the pylon, and flow separation occurs. The rear of the pylon is a sharp corner, and the potential flow increases in velocity before the sharp corner. However, flow separation occurs at the rear of the pylon and changes the actual flow field from a potential representation. In order to remove the effect of the sharp corner in the potential flow field, additional sources were placed in the separated region behind the pylon. The pylon is essentially extended downstream, and the pressure distribution obtained by this approach is shown by the dashed lines in Figure 8. Agreement between test data and theory is now more realistic.

In order to determine the pressure distribution in the separated region on the aft end of the main fuselage, an approach similar to that of the pylon was used. Various source distributions were used in the flow separated region; however, none have been successful in simulating the pressure distribution in this region. Flow separation is an extremely difficult area, and a large effort will be required to solve the problems associated with this phenomenon.

FLOW VISUALIZATION

Top and side views of the fuselage configuration taken during the oil flow studies are presented in Figures 9 and 10. Separation occurs before and around the pylon for all angles of attack. Separation occurring before and around the pylon is probably local rather than the catastrophic type that occurs at the rear of the pylon. Catastrophic separation also occurs at the aft end of the main body where large adverse pressure gradients are encountered. The boundary layer analysis predicted separation between fuselage stations 37 and 39 on the aft end of the main fuselage and foward of the pylon.

BOUNDARY LAYER VELOCITY PROFILES

Test data and theory are compared for the fuselage without pylon at zero angle of attack in Figure 11. The height above the model surface has been nondimensionalized by the boundary layer thickness and the local velocity by the velocity at the edge of the boundary layer. A boundary layer trip was placed at fuselage station 4 to cause transition to turbulent flow at a known location. Thus, profiles measured at fuselage station 3.5 are laminar and the remaining areas are turbulent. The laminar boundary layer thickness is of the order of the probe dimensions, and the test data in this region is questionable. Agreement between test data and theory is generally excellent in the turbulent region. There is no apparent reason for the poor agreement between test and theory on the top centerline at fuselage station 18. There is also poor agreement on waterline 8 at fuselage station 35; however, this is a region of highly three-dimensional flow, and the small cross-flow assumption should not be expected to be valid. The correlation indicates that the small cross-flow assumption is sufficiently accurate over a major portion of the fuselage model.

PARASITE DRAG

Drag versus angle of attack is shown in Figure 12 for the configurations used in the test program. The drag has been divided by the dynamic pressure and is presented as an equivalent area in square feet. The blunt-nosed configuration is the original BO-105 shown in Figure 6. A streamlined nose was designed for the model to provide an alternate configuration, since it was thought that the blunt-nosed BO-105 would have some flow separation on the nose. Although adverse pressure gradients exist on the nose of the BO-105, they are not severe enough to cause flow separation. Analysis later confirmed the test data, in that there was little difference in drag between the two nose configurations.

Test data have been included for the rotor hub and skids to demonstrate the significant contribution of the skids and hub to the total drag. No attempt was made to model the

12

hub or skids analytically; they present a formidable problem and will be the subject of future work. Hubs and skids present an additional problem in that large-scale component testing may be required to provide valid data due to the Reynolds-number problem.

The procedure for determining the drag analytically is as follows:

1. Determine the potential flow field using . Douglas-Neumann program.

2. Determine the fuselage streamlines using the computer program of Reference 3.

3. Determine the boundary layer along streamlines assuming small cross flow using the computer program of Reference 4. This program determines skin friction distribution and points of flow separation.

4. Determine the skin friction drag by summing the skin friction drag contribution on each panel on the potential flow model. Assume zero skin friction drag in the flow separated region.

5. Determine the pressure drag in the attached flow region by summing the pressure drag contribution on each panel on the potential flow model.

Prior to summing the skin friction and pressure drag to determine the parasite drag, one further step is required: determining the pressure drag in the flow separated region. Since the pressure drag due to flow separation cannot be analytically determined yet, an empirical approach based on the test data has been used to demonstrate the accuracy of the drag prediction method. Physically, the area at the base of the fuselage behaves as a pump with an overall negative pressure coefficient. Based on the experimental data, an average pressure coefficient of -0.1 was assumed to represent the separated region for all angles of attack.

Drag predictions using this approach, shown by the solid lines in Figures 13 and 14, are compared to test data. Agreement with test data is very good around zero angle of attack and tends to become poorer at the higher positive and negative angles of attack. This is due to the nature of the assumption of the pressure field in the separated region. The drag was also determined using the actual pressure data obtained from the test program in the separated region. The drag obtained using this approach is shown by the dashed lines in Figures 13 and 14. This represents the level of drag prediction capability that could be obtained if a means of determining the pressure in the separated region could be developed. The following relationship for an average pressure coefficient as a function of angle of attack would approximate the pressure drag of the separated region very accurately:

$$C_p = -.1 + .002\ a$$

where the units of a are degrees.

This relationship yields the same total drag as that obtained by using the test data in the separated region.

13

● DENOTES LOCATION OF BOUNDARY LAYER PROBE
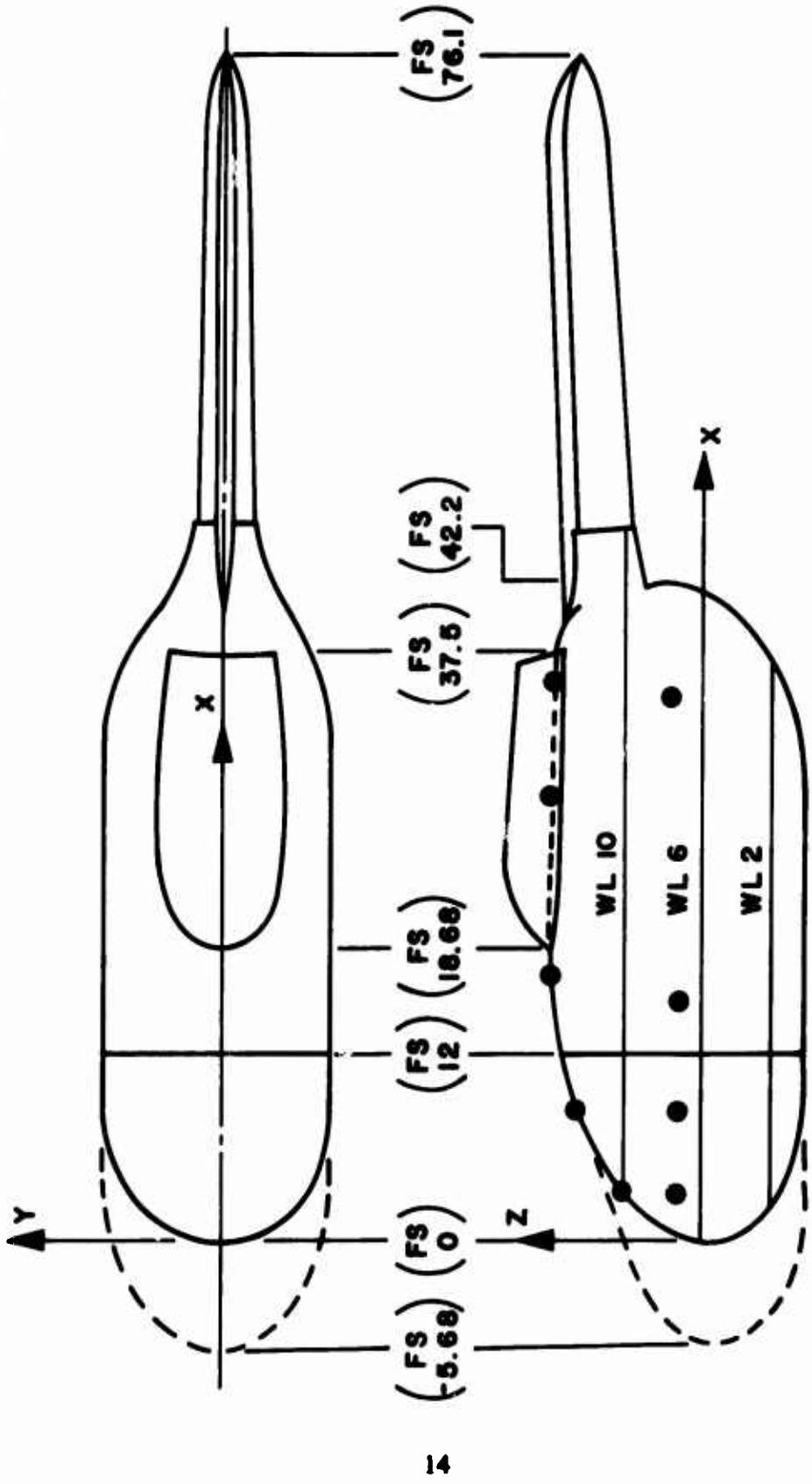
Figure 6. Sketch of BO-105 and Alternate Nose Configuration.

14
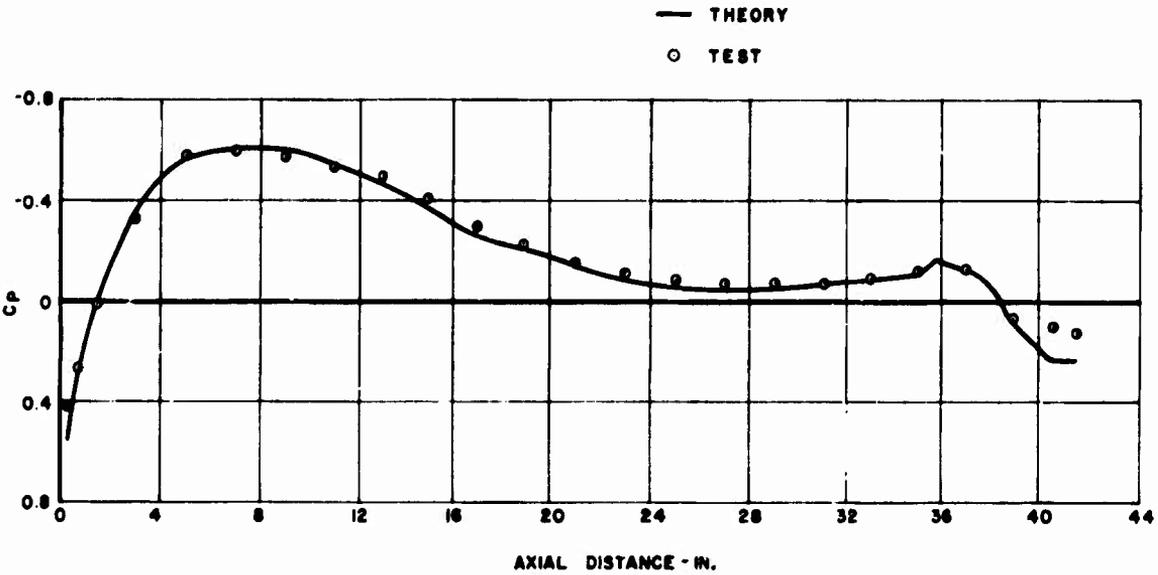
Top Centerline, a = 15 Deg
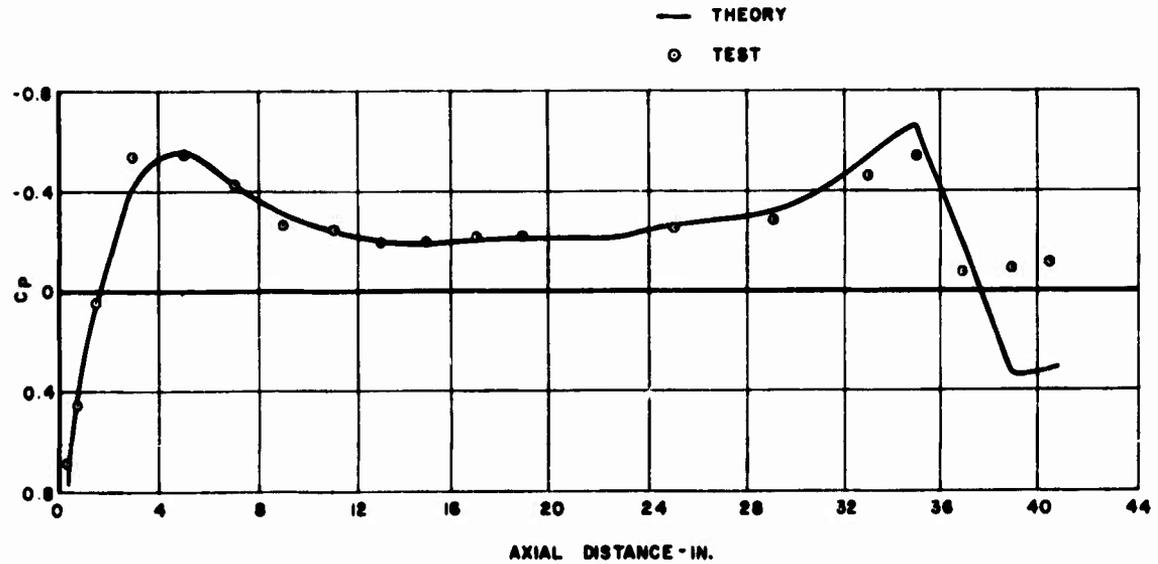
Waterline 6, a = 15 Deg

Figure 7. Pressure Coefficient Versus Axial Distance Without Pylon,
V_∞ = 150 MPH.
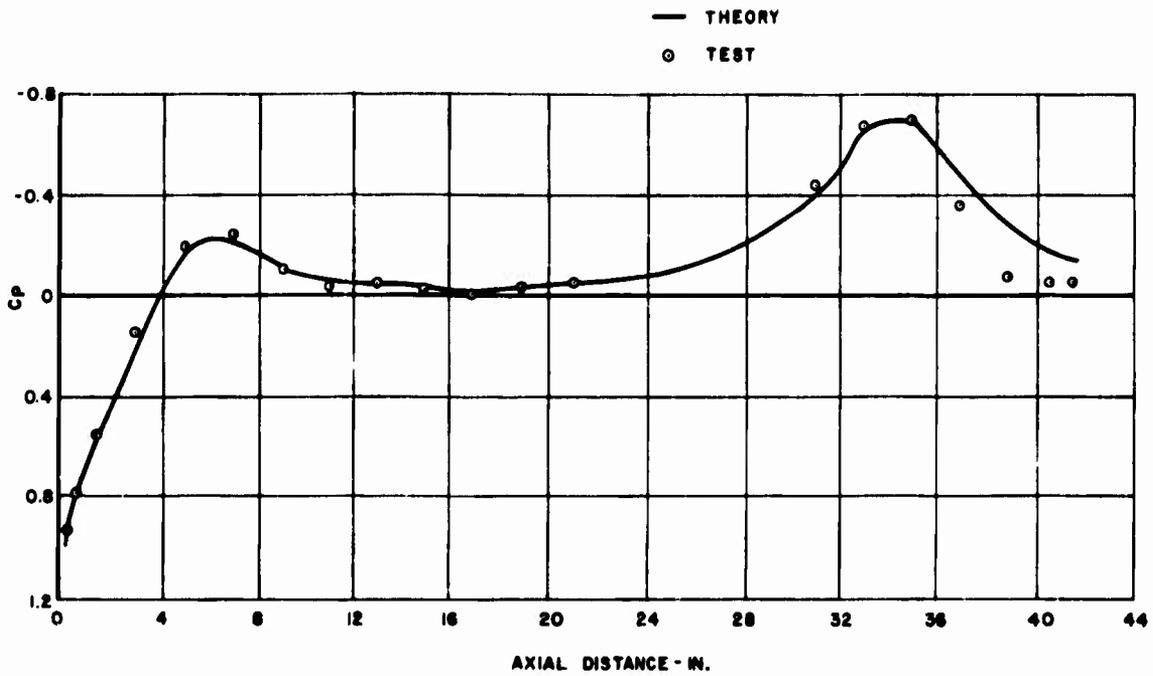
Bottom Centerline, $a = 15$ Deg

Top Centerline, $a = 0$ Deg

Figure 7. Continued.

16
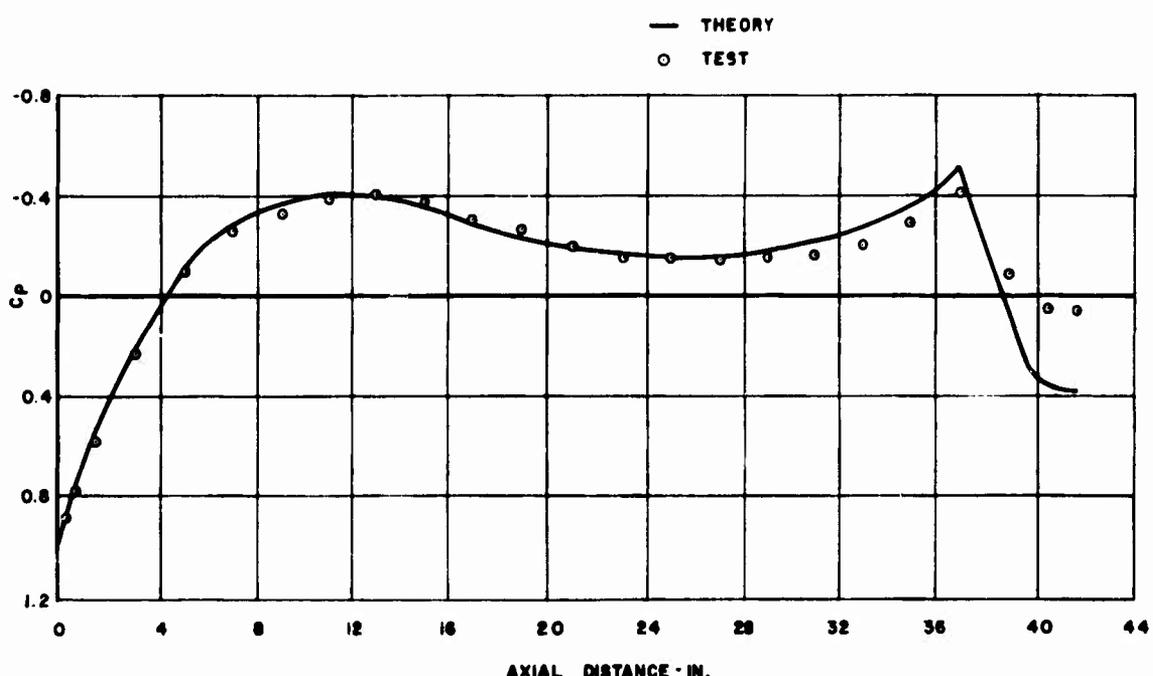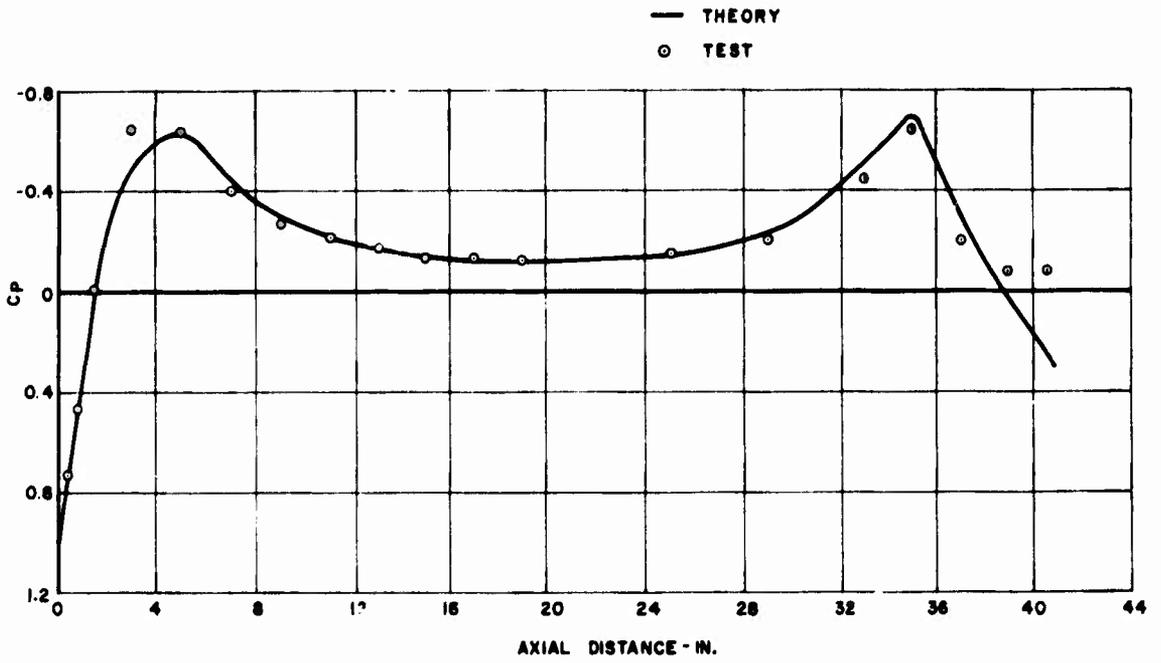
Waterline 6, a = 0 Deg

Bottom Centerline, a = 0 Deg

Figure 7. Continued.

17
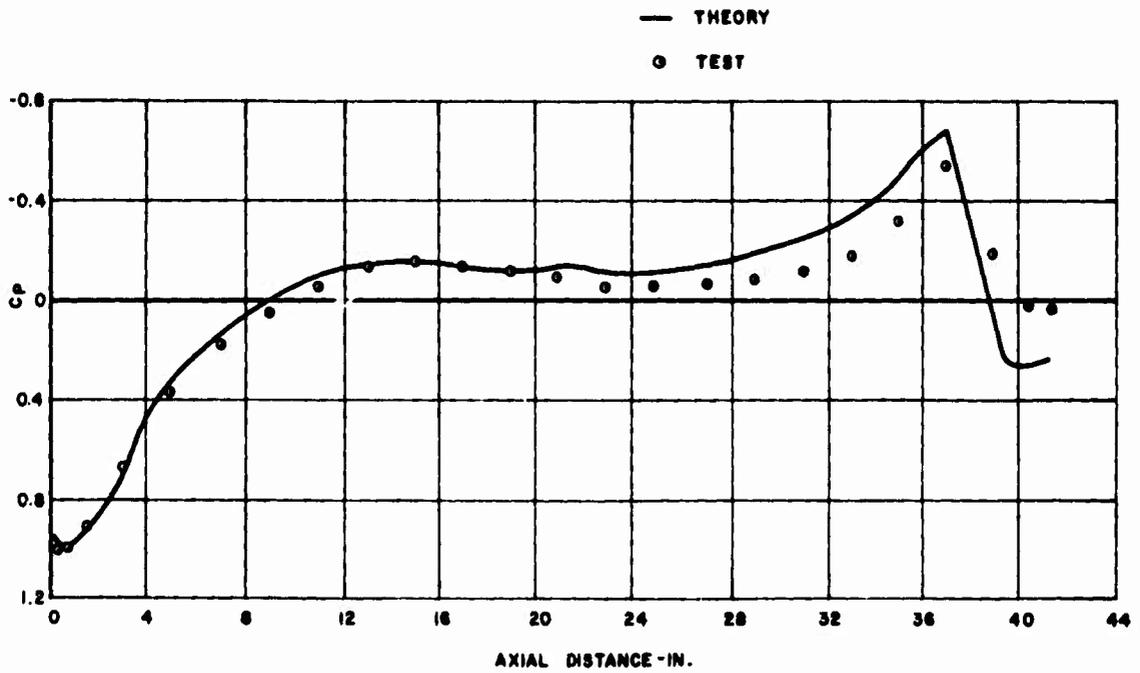
Top Centerline, $a = -15$ Deg
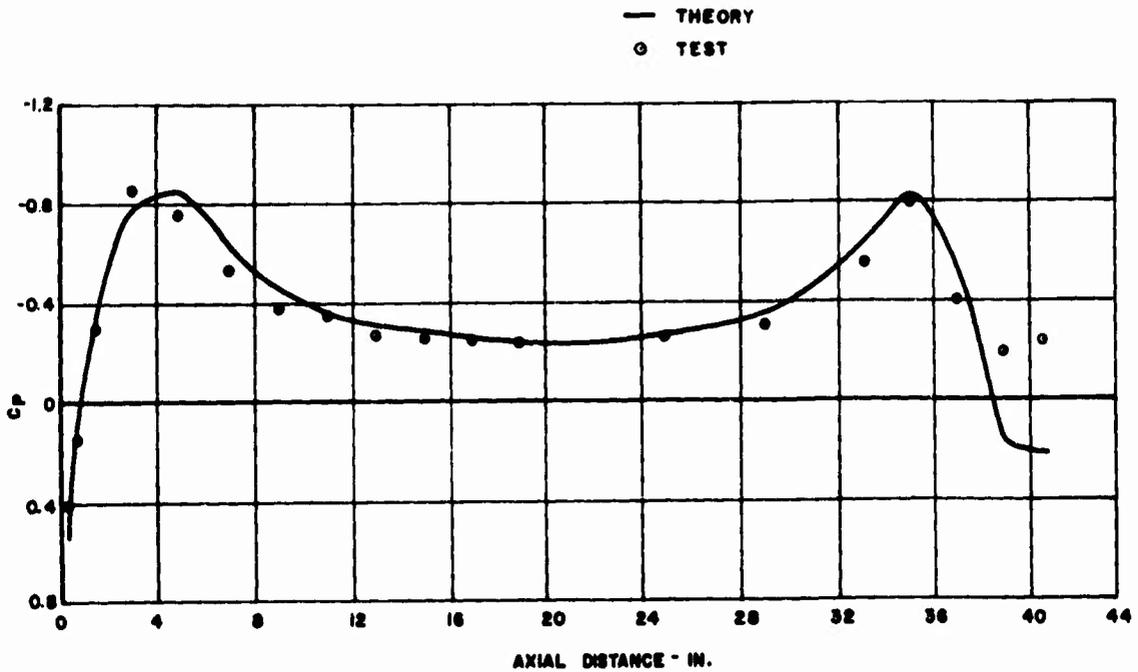
Waterline 6, $a = -15$ Deg
Figure 7. Continued.
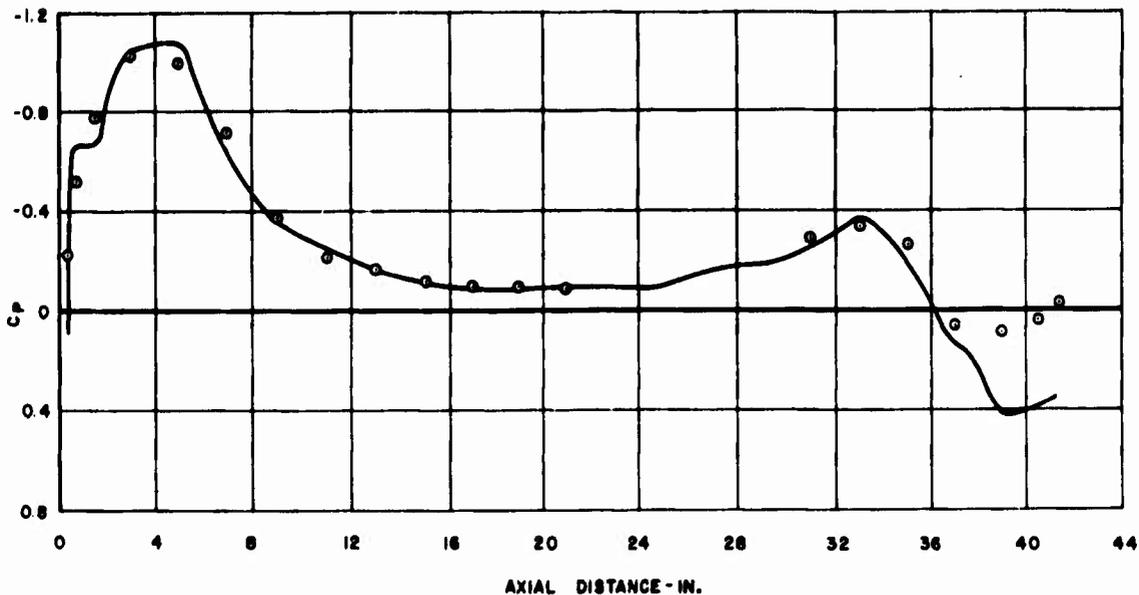
Bottom Centerline, $a = -15$ Deg

Figure 7. Concluded.

THEORY
EXTENDED PYLON
○ TEST
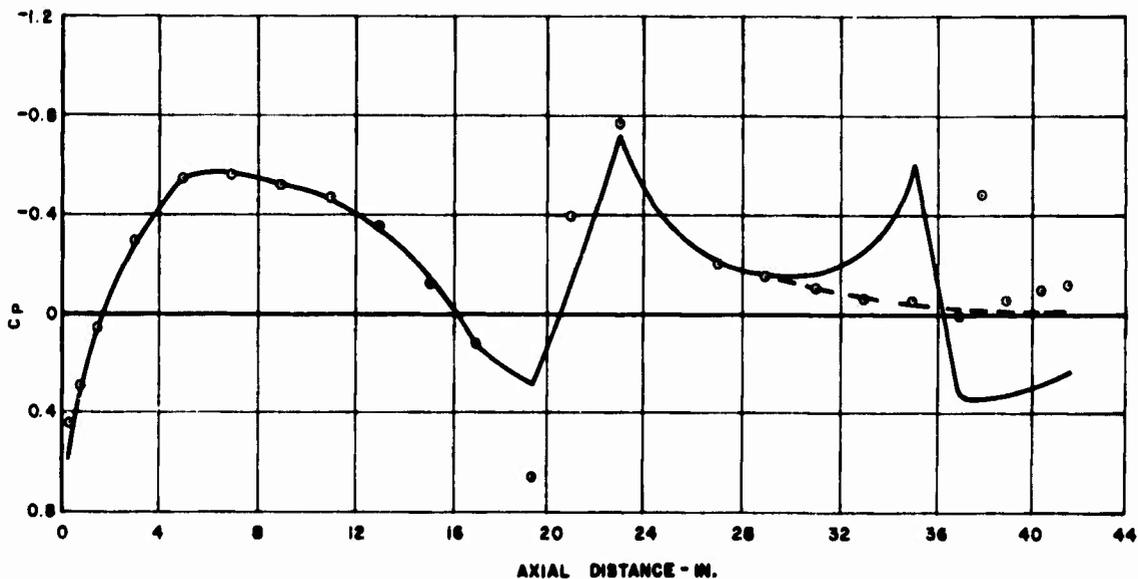
$a = 15$ Deg

Figure 8. Pressure Coefficient Versus Axial Distance on Top Centerline With Pylon,
$V_\infty = 150$ MPH.

$a = 0$ Deg
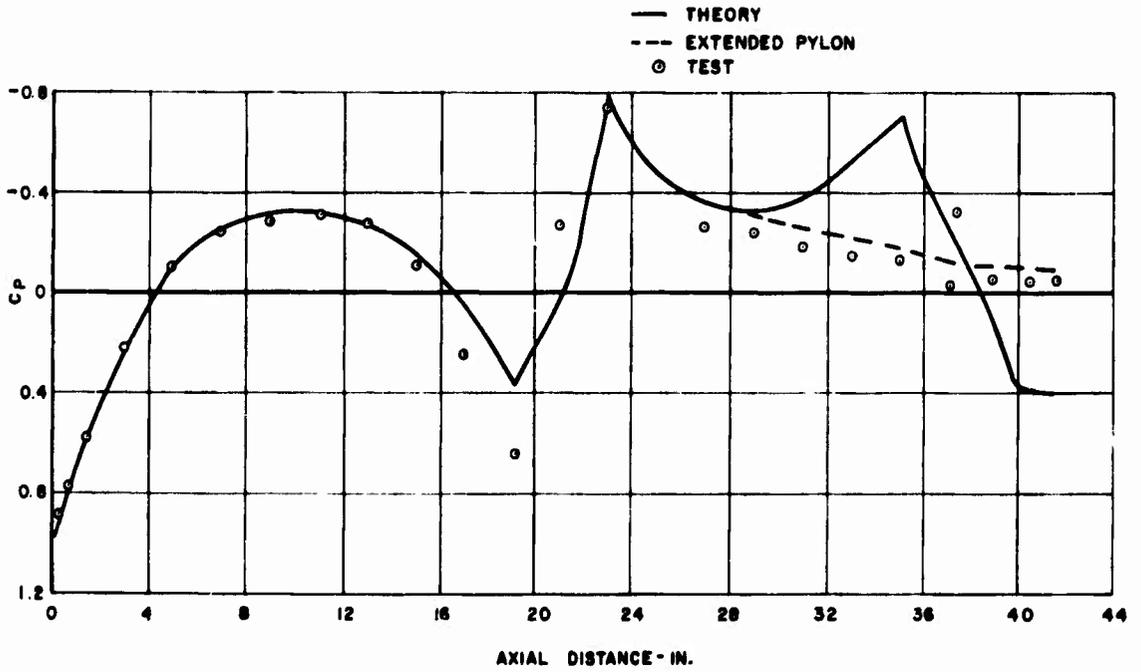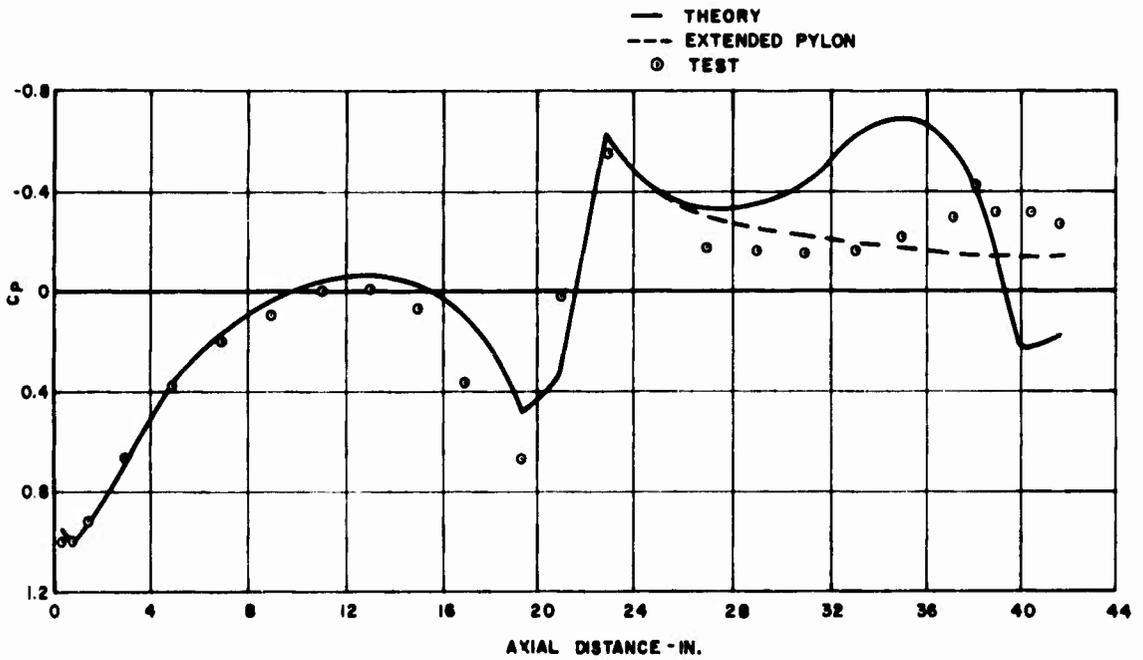
$a = -15$ Deg

Figure 8. Concluded.
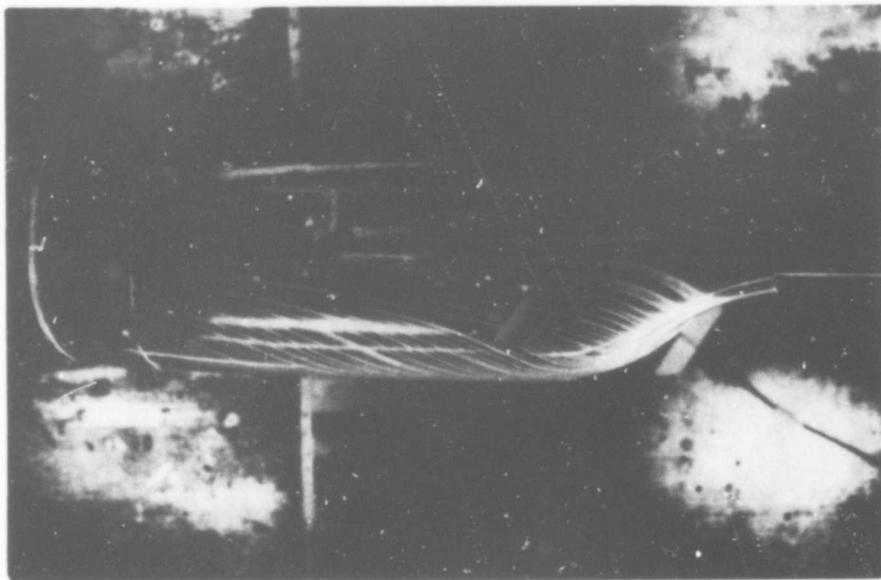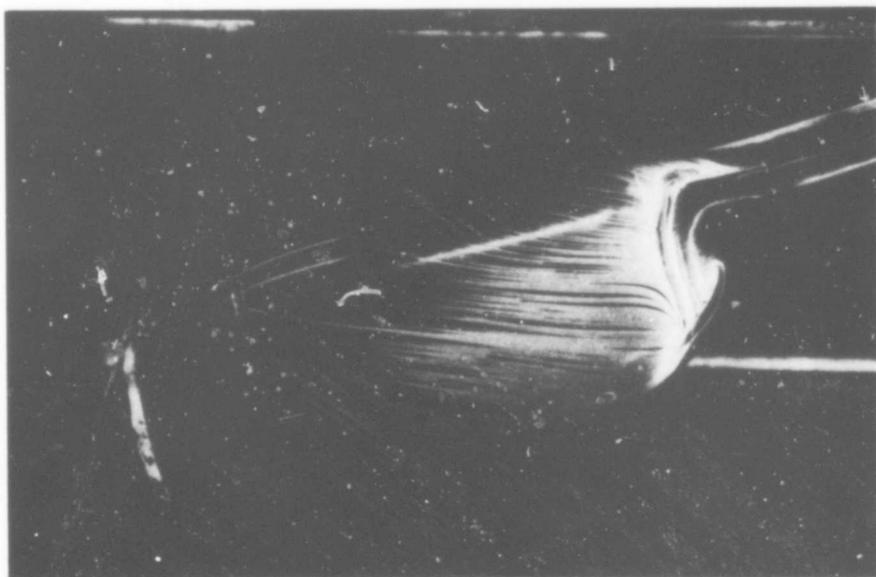
$a = -15$ Deg

Figure 9. Oil Flow Study, Fuselage Configuration Without
Pylon, $V_\infty = 150$ MPH.

21
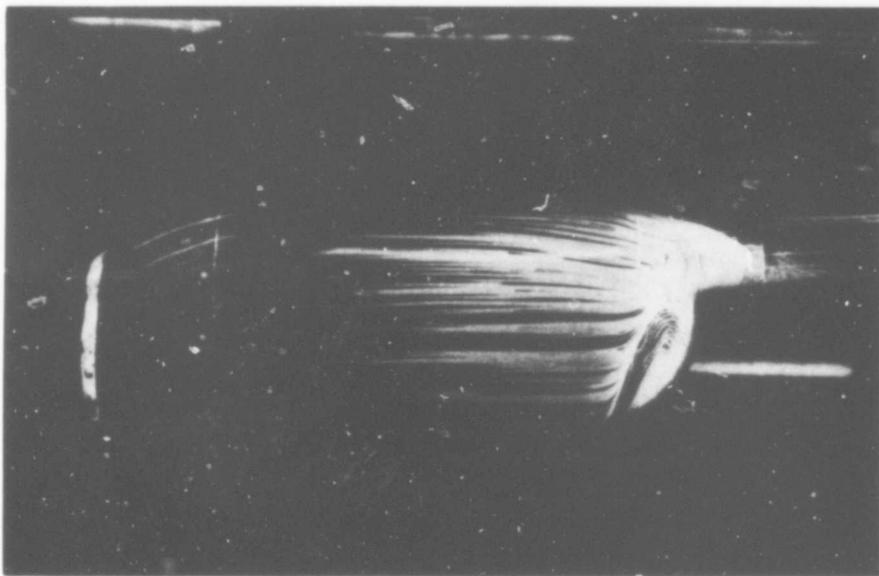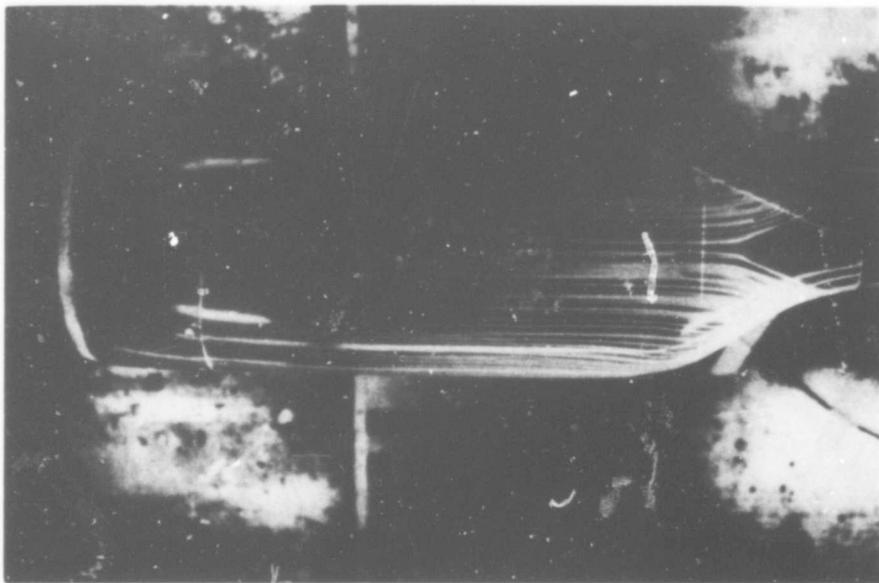
$a = 0$ Deg

Figure 9. Continued.

22
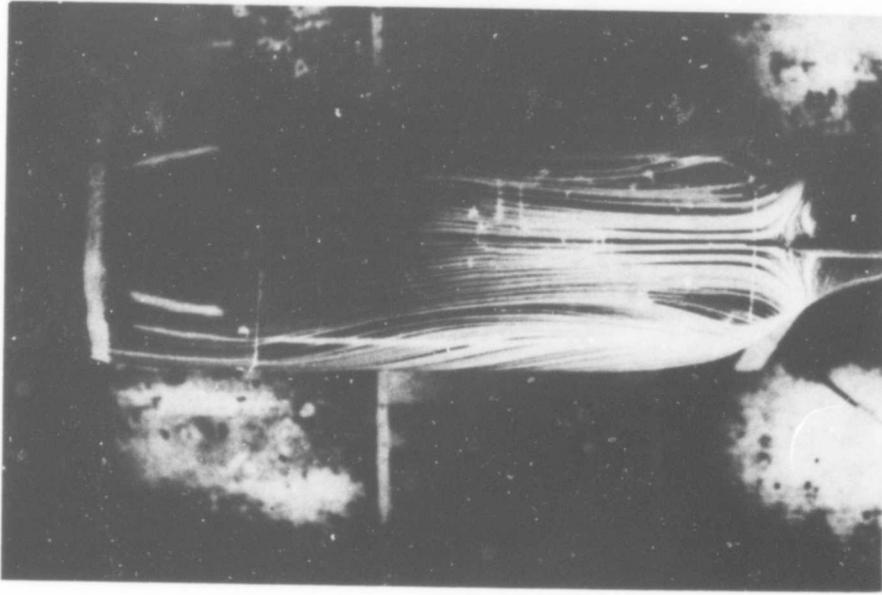
a = 15 Deg

Figure 9. Concluded.

23
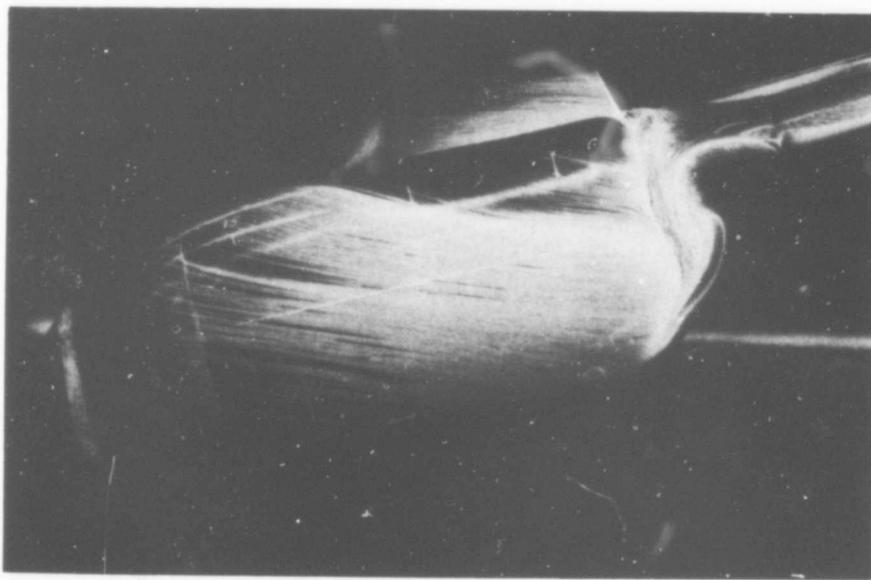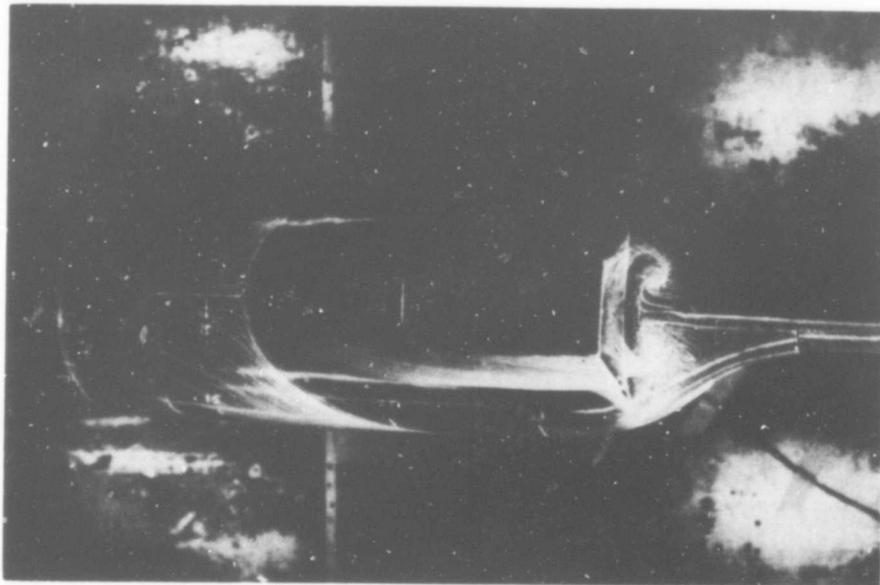
$a = -15$ Deg

Figure 10. Oil Flow Study, Fuselage Configuration With
Pylon, $V_\infty = 150$ MPH.
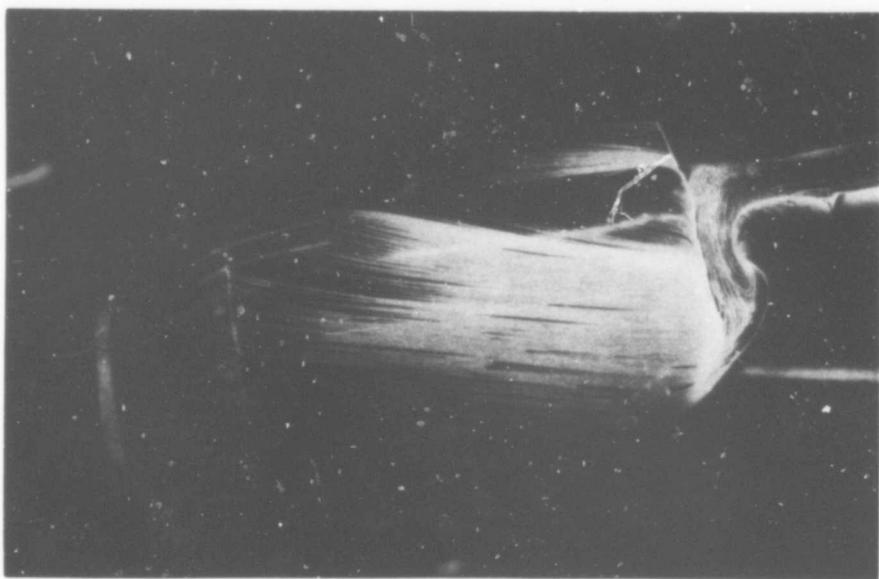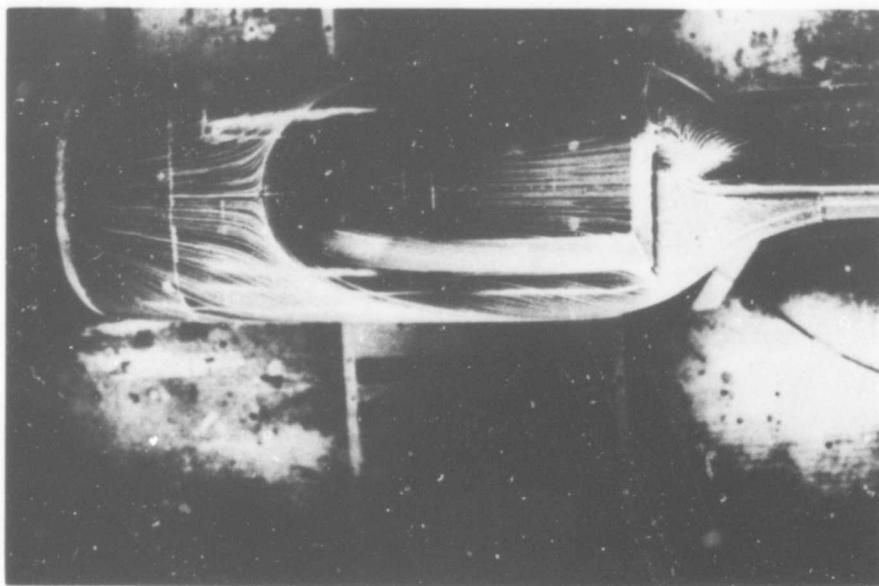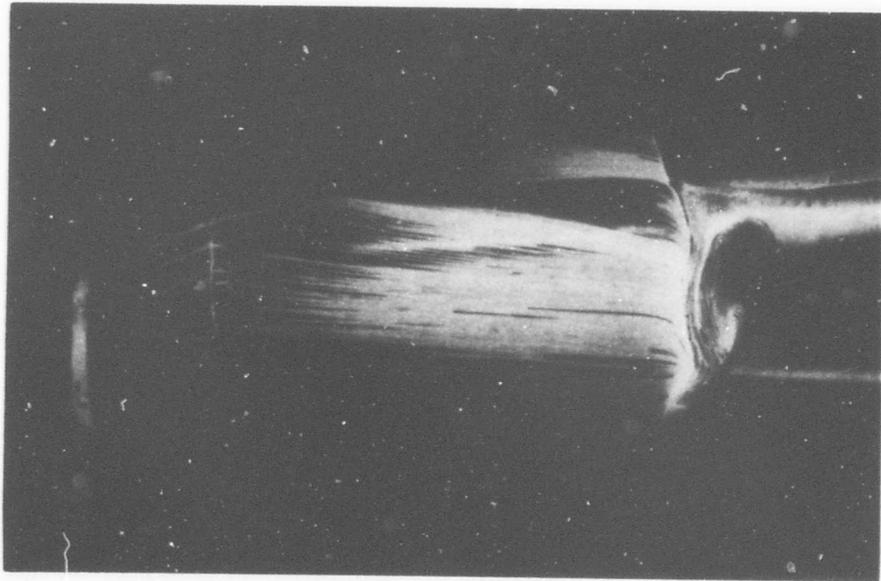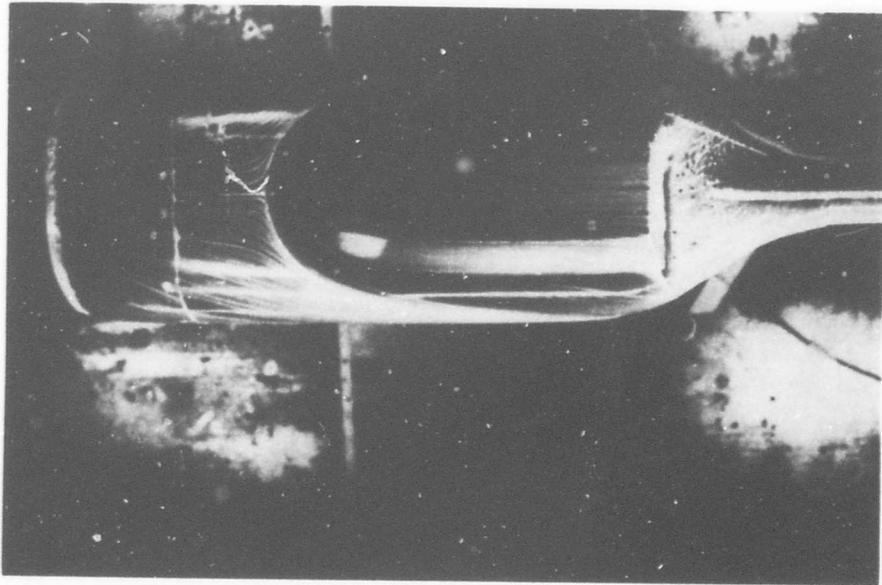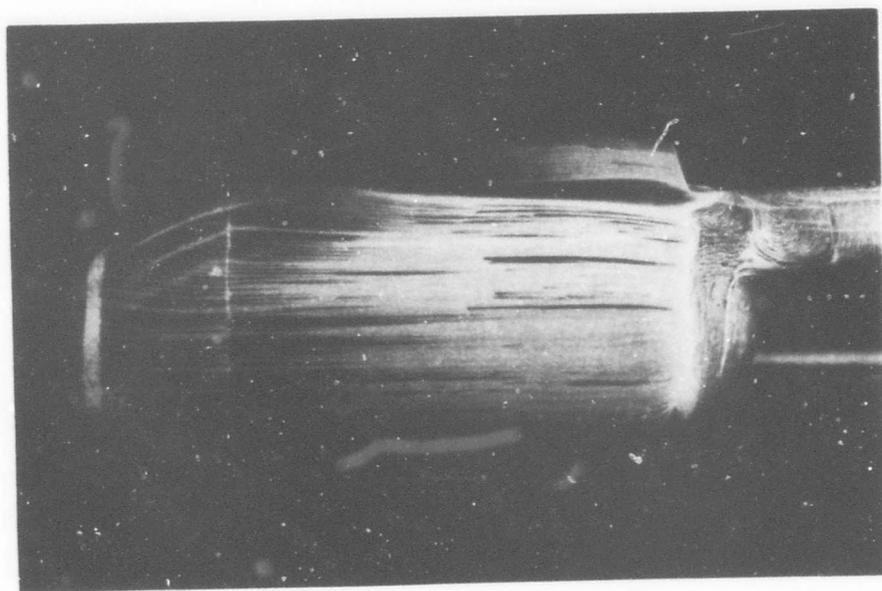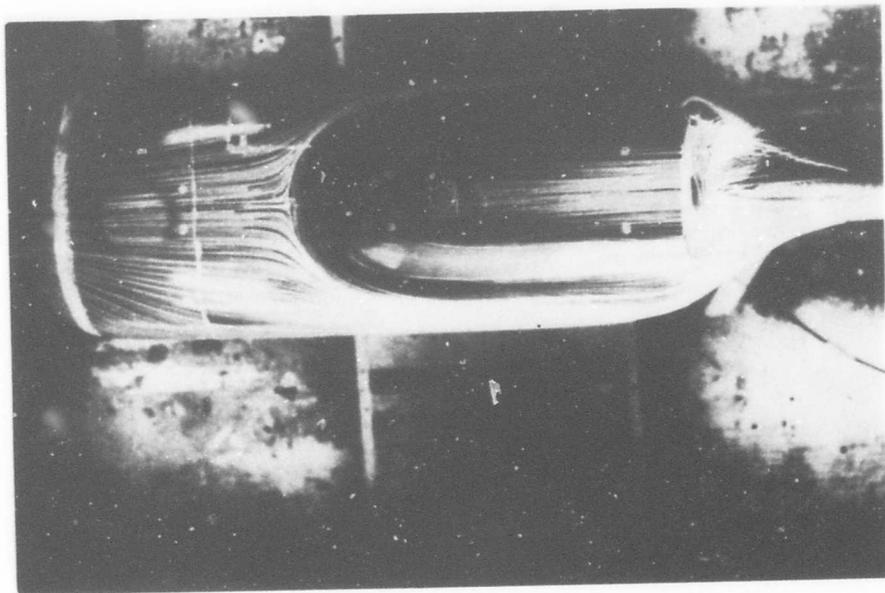
24

$a = -10$ Deg

Figure 10. Continued.

25

$a = -5$ Deg

Figure 10.   Continued.

26

$a = 0$ Deg

Figure 10.   Continued.

27

$a = 5$ Deg

Figure 10. Continued.

28
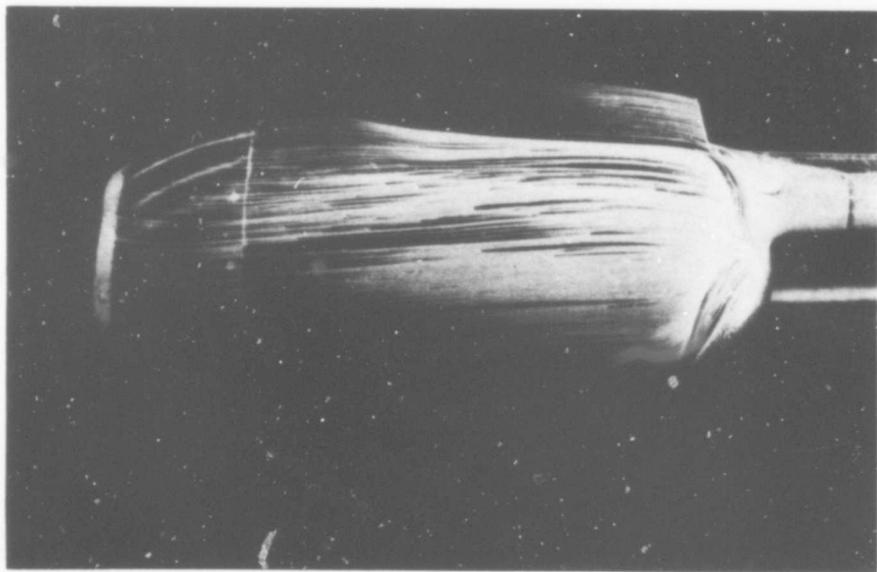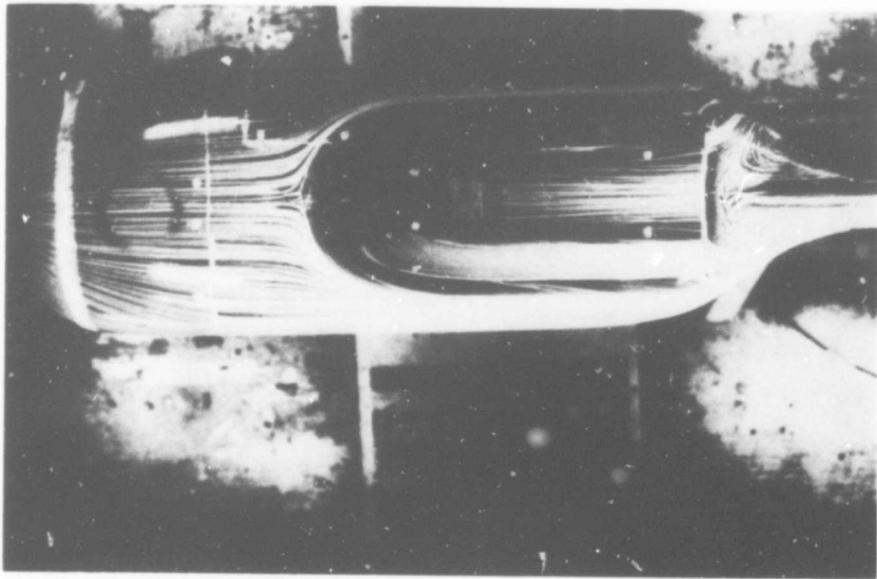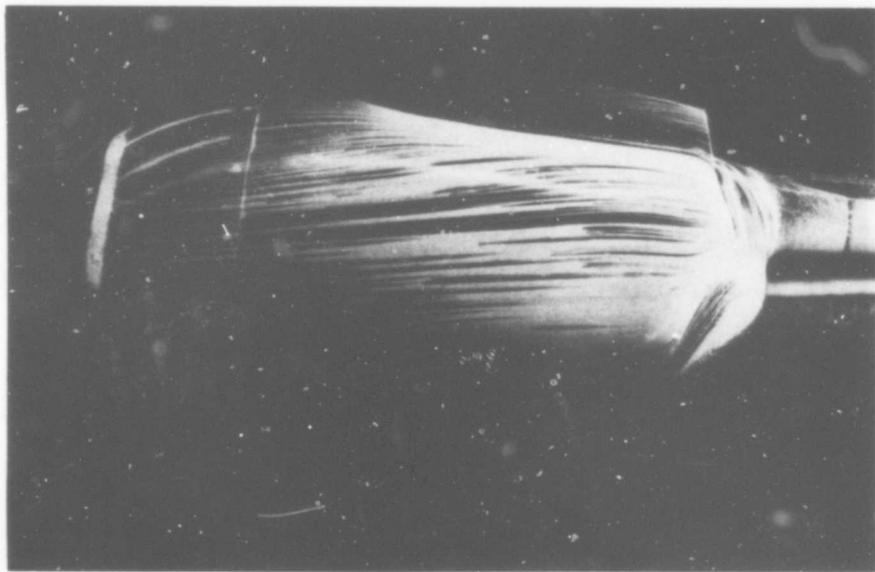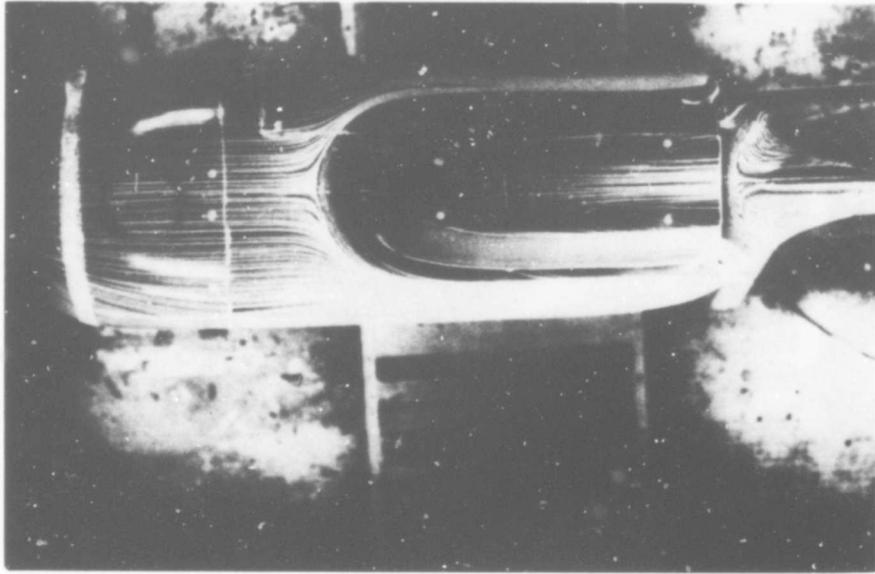
$a = 10$ Deg

Figure 10.   Continued.
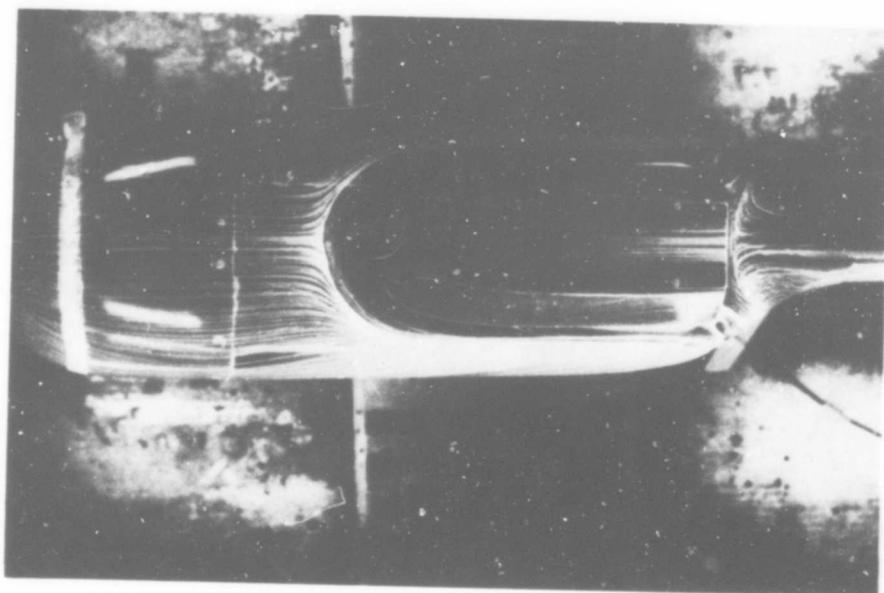
a = 15 Deg

Figure 10. Concluded.
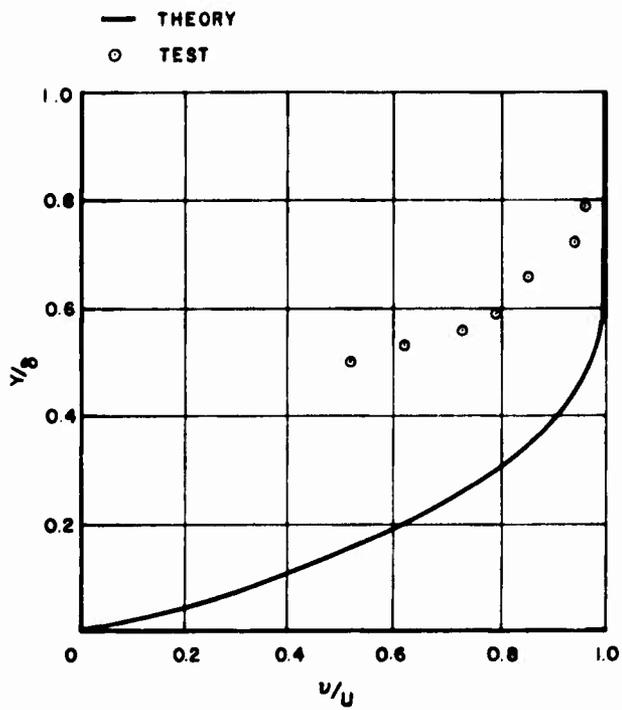
Top Centerline, Fuselage Station 3.5
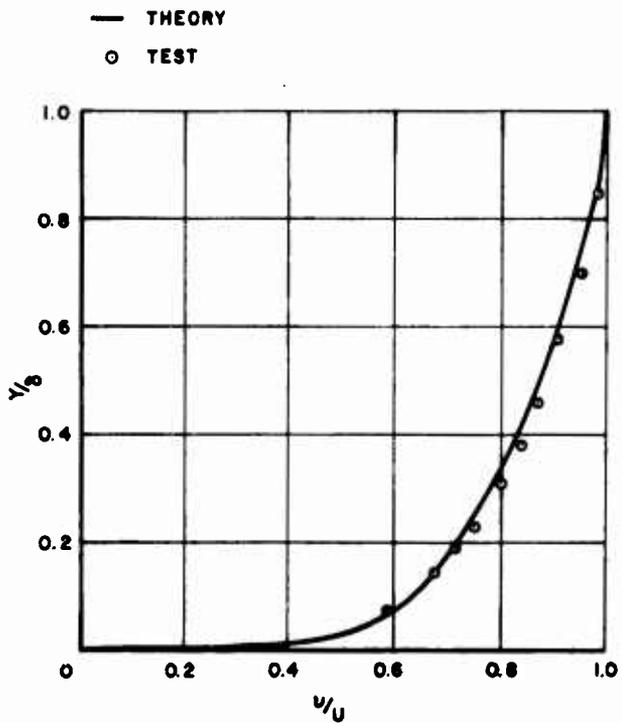
Top Centerline, Fuselage Station 10

Figure 11.   Boundary Layer Velocity Profile; V_∞ = 150 MPH, a = 0 Deg.
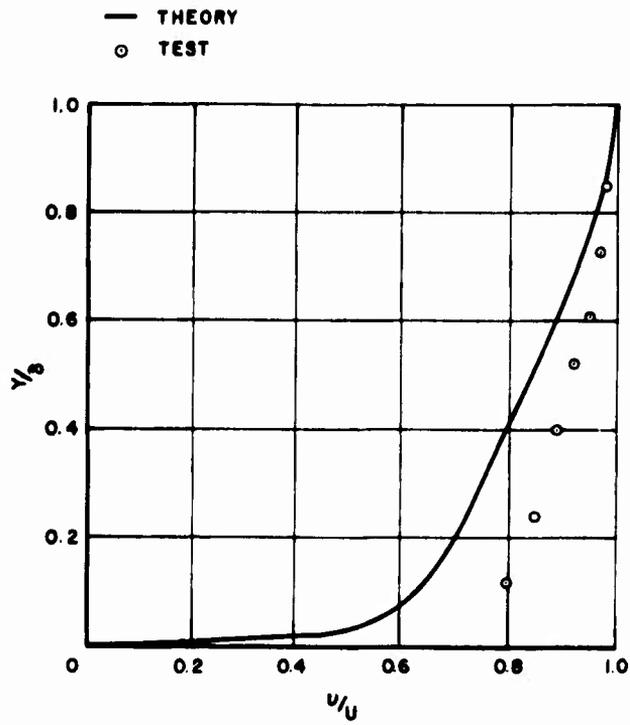
Top Centerline, Fuselage Station 18
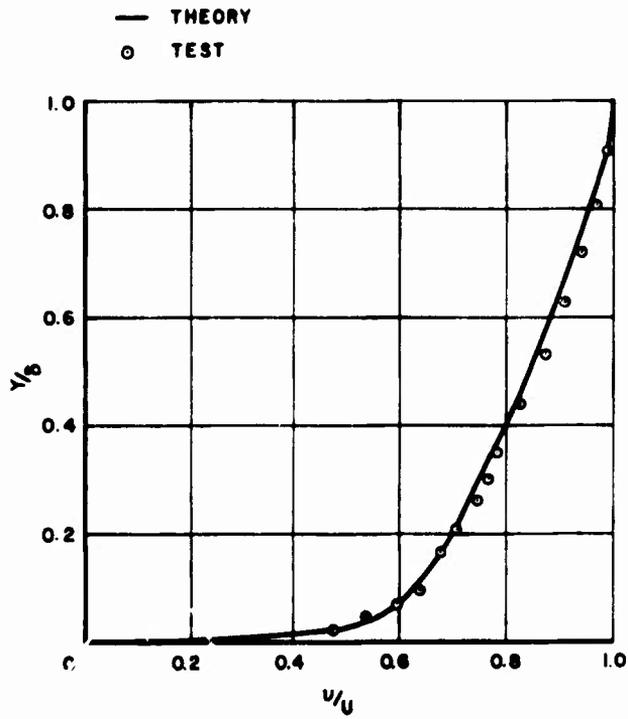
Top Centerline, Fuselage Station 28
Figure 11. Continued.

32
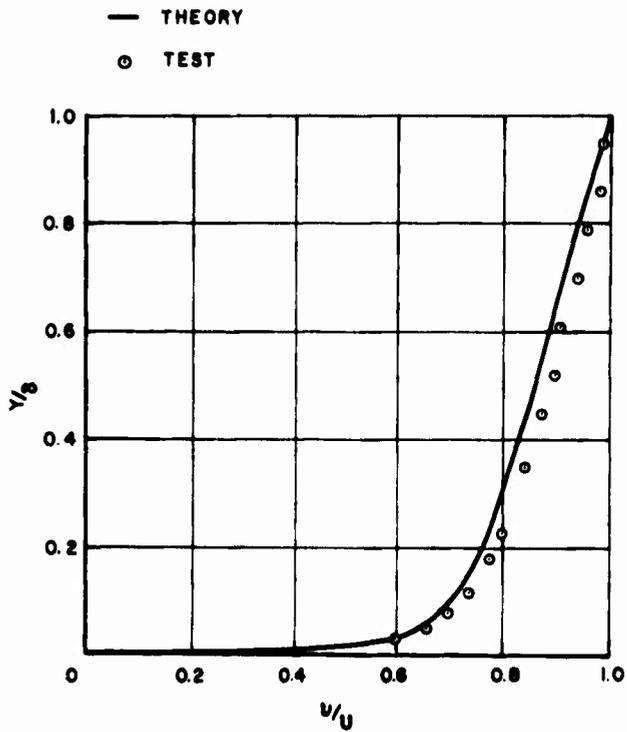
Top Centerline, Fuselage Station 36
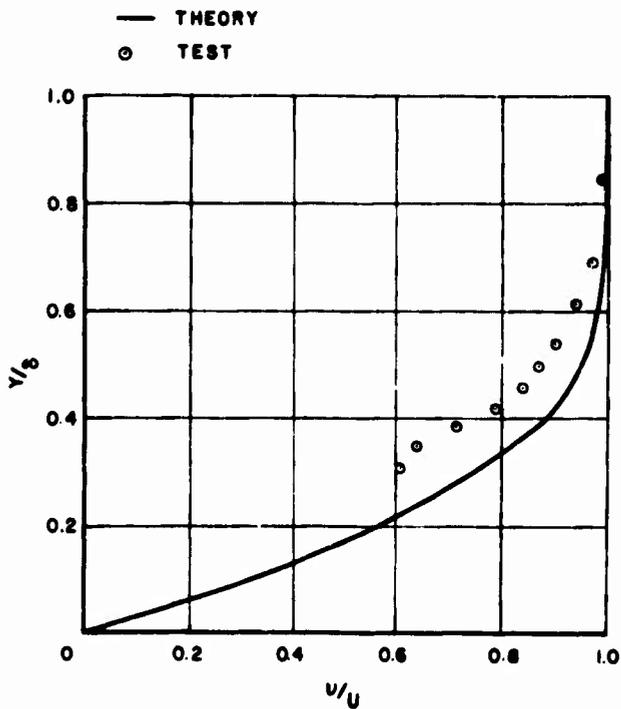
Waterline 8, Fuselage Station 3.5
Figure 11. Continued.

33
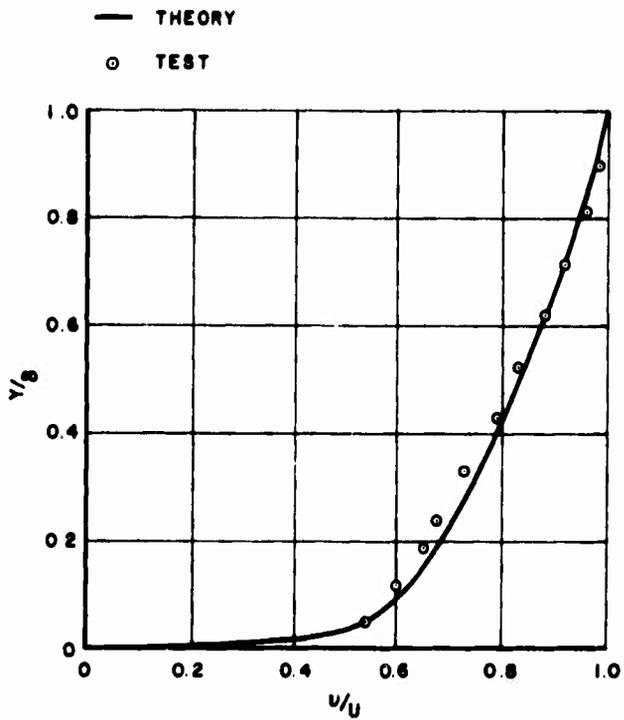
Waterline 8, Fuselage Station 10
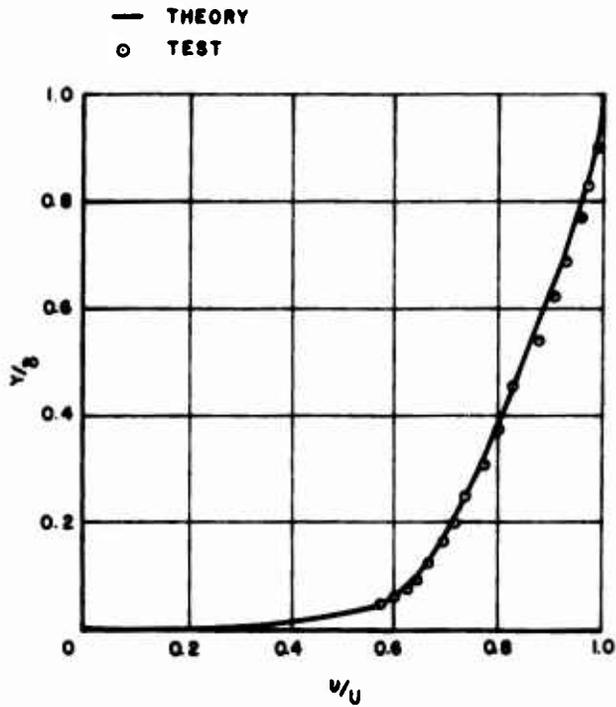
Waterline 8, Fuselage Station 16
Figure 11. Continued.

34

THEORY

o TEST
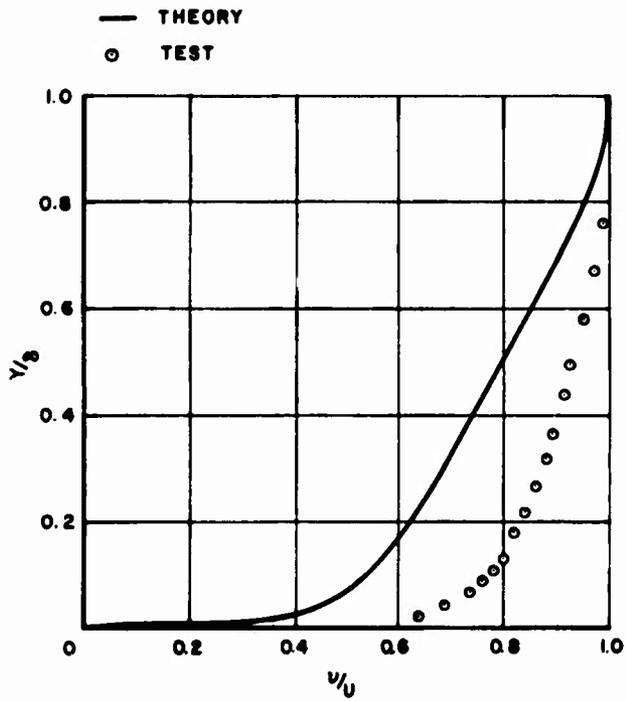
Waterline 8, Fuselage Station 35

Figure 11. Concluded.

35
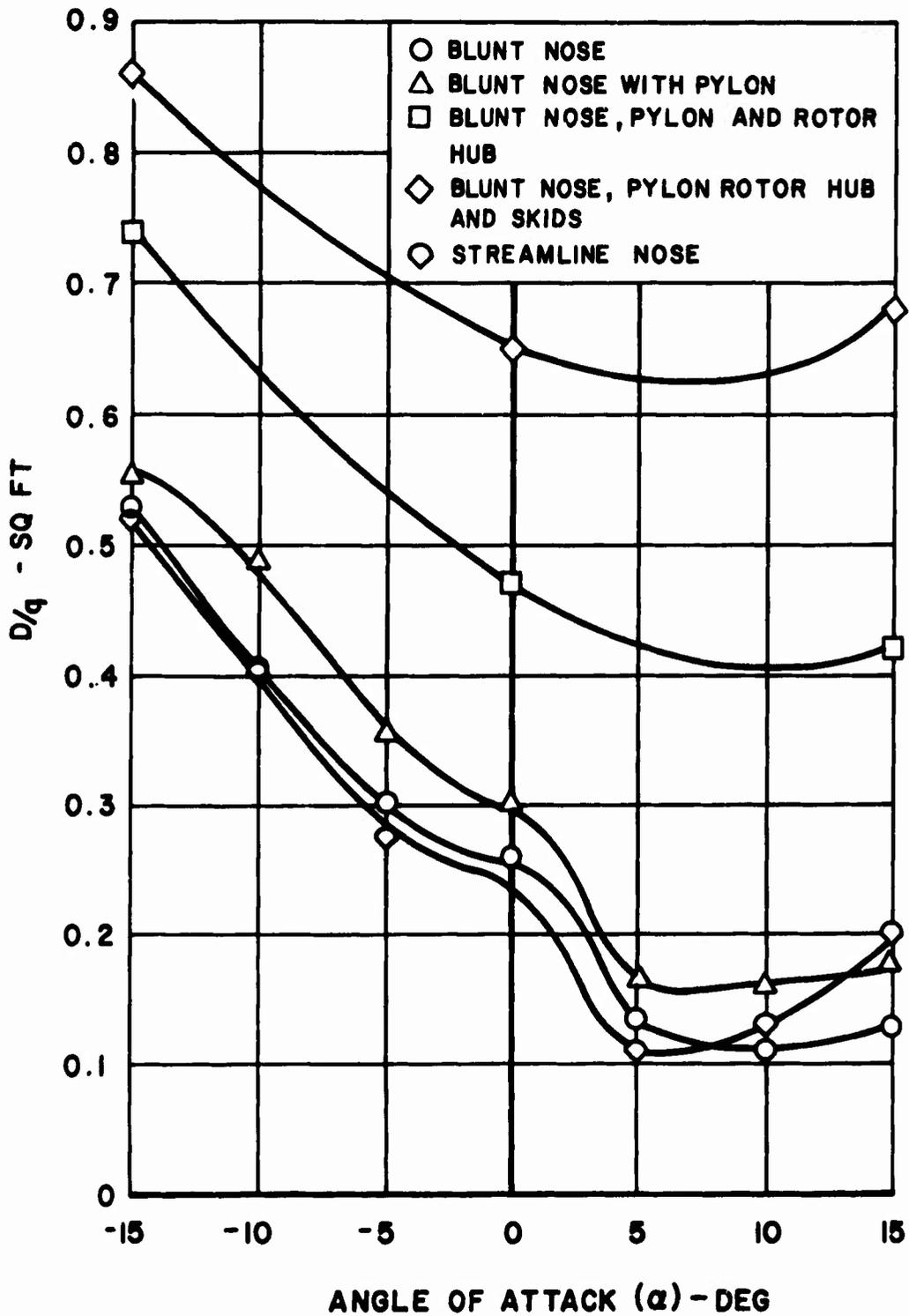
Figure 12. Drag Versus Angle of Attack, V∞ = 150 MPH.
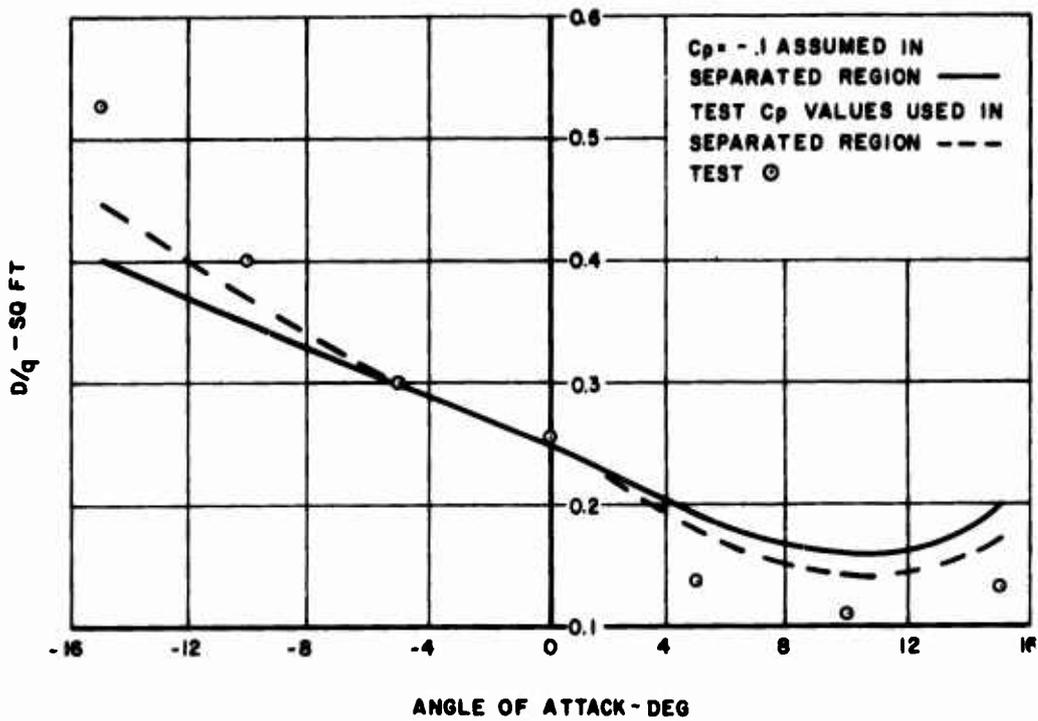
Figure 13. Drag Versus Angle of Attack on Fuselage Without Pylon,
$V_\infty \approx 150$ MPH.
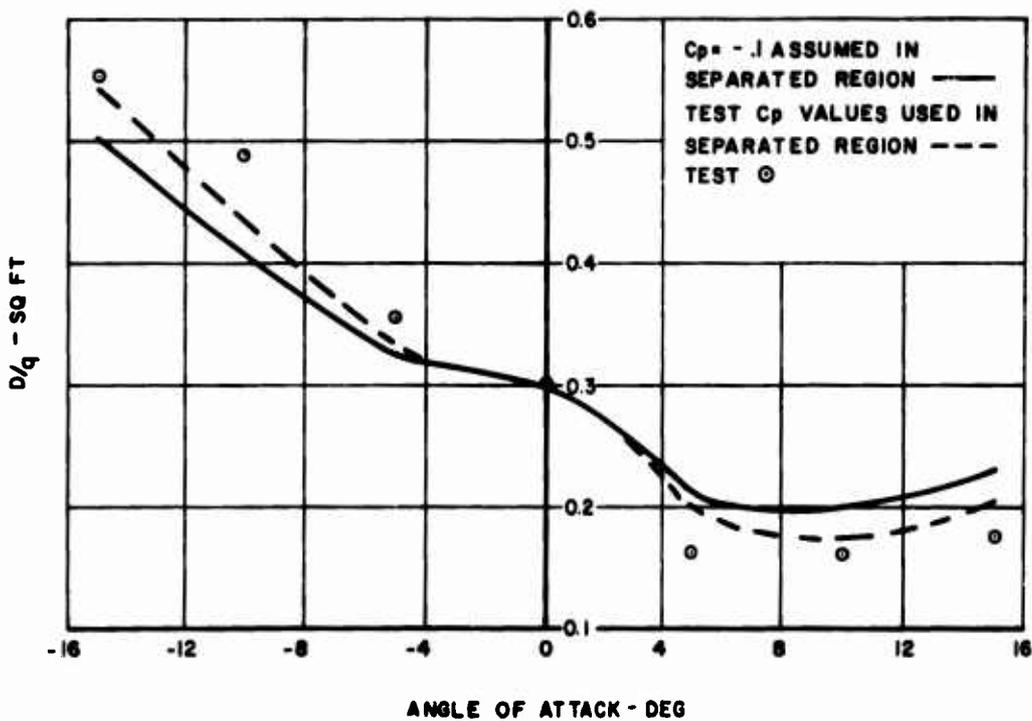
Figure 14. Drag Versus Angle of Attack on Fuselage With Pylon,
$V_\infty = 150$ MPH.

37

CONCLUSION

The application of advanced analytical methods to the prediction of fuselage drag has been demonstrated. Results indicate that reasonable drag predictions can be made if a means of determining the pressure in the separated region can be developed. This work represents a first cut at an extremely difficult problem. Two immediate applications of this procedure are evident. The method can be used in the design of fuselages of minimum parasite drag. Alternate fuselage configurations can be investigated to determine the one with the least flow separation, thus minimizing the drag. The second immediate use is to provide pressure data on the fuselage for structural design purposes.

LITERATURE CITED

1. Hoerner, Sighard F., FLUID DYNAMIC DRAG, Published by Author, 1965.

2. Hess, John L., and Smith, A. M. O., CALCULATION OF NON-LIFTING POTENTIAL FLOW ABOUT ARBITRARY THREE-DIMENSIONAL BODIES, Douglas Aircraft Co. Report No. E. S. 40622, Douglas Aircraft Co., Long Beach, California, 15 March 1962.

3. DeJarnette, Fred R., CALCULATION OF INVISCID SURFACE STREAMLINES AND HEAT TRANSFER ON SHUTTLE TYPE CONFIGURATIONS, NASA CR-111921, National Aeronautics and Space Administration, Washington, D. C., August 1971.

4. Price, Joseph M., and Harris, Julius E., COMPUTER PROGRAM FOR SOLVING COMPRESSIBLE NONSIMILAR-BOUNDARY-LAYER EQUATIONS FOR LAMINAR, TRANSITIONAL, OR TURBULENT FLOW OF A PERFECT GAS, NASA TMX-2458, National Aeronautics and Space Administration, Washington, D. C., April 1972.

5. Linville, James C., AN EXPERIMENTAL INVESTIGATION OF HIGH-SPEED ROTORCRAFT DRAG, USAAMRDL Technical Report 71-46, Eustis Directorate, U. S. Army Air Mobility Research and Development Laboratory, Fort Eustis, Virginia, February 1972, AD 740771.

APPENDIX
UNIVERSITY OF MARYLAND TEST PROGRAM

MODEL DESIGN

A ¼-scale fiberglass model of the BO-105 was selected for the test program. An alternate streamline-nosed configuration was also designed. The streamlined nose was 5.67 inches larger than the blunt-nosed BO-105 and was faired into the fuselage at model station 12 (see Figure 6). In addition to the two nose shapes, a pylon, skid landing gear, and rotor hub were used in the test program.

MODEL FABRICATION

Plaster molds were made of a ¼-scale model of the BO-105 to be used to construct the fiberglass shell model. The shell was laid up in the molds in two halves. The nose portions of the halves were made first, trimmed off at fuselage station 12, and put back into the models. The remaining halves of the model were then laid up with a lip overlapping the nose pieces, thereby making the nose pieces separate from the main body pieces. For the streamlined nose, a wooden model was constructed from which molds were made for the fiberglass layup. This nose was made in two halves and cut off at fuselage station 12 to be interchangeable with the blunt nose.

Prior to joining the components together, fore and aft bulkheads were secured to the main fuselage halves. These bulkheads were the main load-carrying members. They were bolted to a steel box that was connected to the model support through a remote-controlled pitch mechanism. A cutout was also provided on one side for access to the inside of the model.

The tail boom was cut off just forward of the BO-105 vertical fin and faired off with a wooden plug.

The pylon, which was also made of fiberglass, was in one piece and could be attached to the main fuselage with machine screws.

Landing skids were constructed from tubing and attached directly to the bulkheads in the model. The rotor hub was borrowed from the BO-105 model. The skids, pylon, and rotor hub are shown installed on the blunt-nosed configuration in Figure 15.

PRESSURE ORIFICES

To obtain sufficient data on the pressure distribution over the model surface, a large number of pressure orifices were required. For the basic fuselage and components, 265 pressure taps were provided. The locations of the individual orifices are shown in Tables I through IV.

Positions of the pressure orifices were located and drilled on the model surface. A short length of 0.064 stainless steel tubing (approximately 1.5 inches long) was inserted in each hole flush with the outer surface, bonded in place with an epoxy patching adhesive, and

connected to a pressure scanning valve by plastic tubing. Forty-eight tubes were connected to each of five scanning valves.

BOUNDARY LAYER SURVEY MECHANISM

Boundary layer velocity profiles at ten locations on the model for three different model configurations were desired. To achieve this number of velocity profiles in a reasonable amount of testing time, it was necessary to design and construct a boundary layer probe traversing device. The device was designed around a motor that could be stepped by electrical pulses to move the probe vertically from the surface at the rate of 0.0001 inch per pulse. The traversing mechanism was mounted at ten locations in the model as follows:

1. Five locations along the top centerline at fuselage stations 3.5, 10, 18, 28, and 36.

2. Five locations on the side along waterline 8 at fuselage stations 3.5, 10, 16, 22, and 35.

Figure 16 shows the traversing mechanism mounted in the blunt nose.

A special probe was constructed for the boundary layer measurements. Since a very thin laminar boundary flow would exist at station 3.5, the probe was made as small as possible while maintaining reasonable pressure response times. A piece of 0.032-inch stainless steel hyperdermic tubing (flattened to make the tube smaller in the direction of the velocity gradient) was used for the tip of the probe. The probe was constructed to the small probe dimensions shown in Figure 17. The overall probe height of 0.012 inch was adequate for determining boundary layer thickness.

TEST FACILITY

The model tests were conducted at the University of Maryland subsonic wind tunnel test facility. The tunnel has a rectangular test section 11 feet wide, 7.75 feet high, and 14 feet long. Allowing for the 45-degree corner fillets, the test section cross-sectional area is 84.88 square feet. Tunnel speed is variable over a range of 5 to 235 mph.

The wind tunnel is equipped with a six-component balance system. Load ranges of the balances are:

> Lift: ±5000 pounds
> Drag: ±500 pounds
> Side force: ±1000 pounds
> Pitching moment: ±1000 foot-pounds
> Yawing moment: ±1000 foot-pounds
> Rolling moment: ±1000 foot-pounds

Resolution of the balance system is:

> Lift: ±0.50 pound
> Drag: ±0.10 pound

41

Side force: ±0.10 pound
                    Moments: ±0.20 foot-pound

This resolution applies to loadings of less than 10 percent of forces and 20 percent of
moments. Loadings in excess of these values can be resolved within one-tenth of 1
percent. There are no appreciable interactions in the balance system.

DESCRIPTION OF TESTS

Force and Moment Tests

Force and moment data were recorded at the same time that pressure distribution data
were recorded. For these tests, the model was mounted in the test section on a single
support strut which was attached to the balance system and could be rotated to change
the angle of yaw of the model. Pitch angle was varied using an internal pitch mechanism.
Prior to installing the model on the support strut, loads were applied to the strut to
check the drag balance calibration and the alignment of the strut.

Runs were made to determine the tare and interference effects of the support strut by
inverting the model and running tests with and without a mirror image of the support
strut and fairing installed. The differences between data with and without the image
system installed were taken as the tare and interference effects of the support strut.
Tare and interference runs were conducted for the streamline-nosed configuration and for
the blunt-nosed configuration with and without the skid landing gear. Electrical cables
required for the scanning valves, transducers, and pitch mechanism were routed out of
the model and down the rear of the support strut. The cables were duplicated on the
image strut to account for their tare and interference effects.

In order to pitch the model, a slot was required where the support strut pierced the
model surface. To eliminate interference effects on the force and moment data and
pressure data, this slot was sealed for each setting of angle of attack. For a given run,
the angle of attack was set, the slot was sealed, and the run was made by varying the
angle of yaw. For the tare and interference runs, the slots for the main support and
image strut were both sealed. This eliminated slot effects and ensured that there was
no flow through the model.

In order to improve the correlation between the experimental data and the analytic
method calculations, it was desired to fix transition on the model 4 inches from the
nose. A transition strip was made on each nose shape, 4 inches from the leading edge,
by spraying a 1-inch strip with spray adhesive and sprinkling lightly with carborundum
grit. It was determined that a grit size of 0.0138 inch was suitable to provide transition
at the strip. A quick check in the tunnel indicated that transition begins at the strip
and is complete about ¼ inch aft of the strip.

Pressure Distribution Tests

The pressure distributions were run in conjunction with the force and moment tests. By
mounting the scanning valves and transducers inside the model, it was only necessary to
bring out electrical leads and reference pressure leads. The first three tubes on each valve
were used for reference pressures. Tubes 1 and 2 were wind tunnel reference pressures

used to determine dynamic pressure, q. Tube 3 was used for the test section static pressure.

Using this system, each scanning valve with its associated transducer contained the information necessary to calculate pressure coefficients ($\Delta p/q$). Since the coefficients were ratios of reading from the same transducer, it was not necessary to calibrate the transducers.

Pressure data were recorded on the inverted runs and inverted-plus-image-system runs. The configuration tested and angle ranges covered for the pressure runs were the same as those specified for the force and moment runs. When the model was inverted it was necessary to remove some of the tubes along the top centerline to install the model support. Fortunately, this was an area of relatively constant pressure, so the loss was not significant.

Boundary Layer Traverses

Boundary layer traverses were begun at fuselage station 3.5 on the blunt-nosed configuration. This location was just forward of the transition strip, so it was anticipated that the boundary layer would be quite thin. In order to reduce the response time, a larger probe was constructed for the traverse, aft of the transition strip where the boundary layer would be thicker. The dimensions of the new probe are shown in Figure 17.

Flow Visualization Tests

Flow visualization studies were made using a fluorescent oil technique where a fluorescent powder is mixed in a lightweight motor oil and painted on the model. As the tunnel is brought up to speed, the oil aligns itself with the flow direction on the surface of the model. The model is illuminated with ultraviolet light, causing the powder to fluoresce. Photographs can be taken of the flow pattern using regular black and white film with a suitable filter on the camera.

TEST PROGRAM

The test program is presented in Table V. This table shows the configurations tested, the type of data recorded for each test, and the conditions of each test.
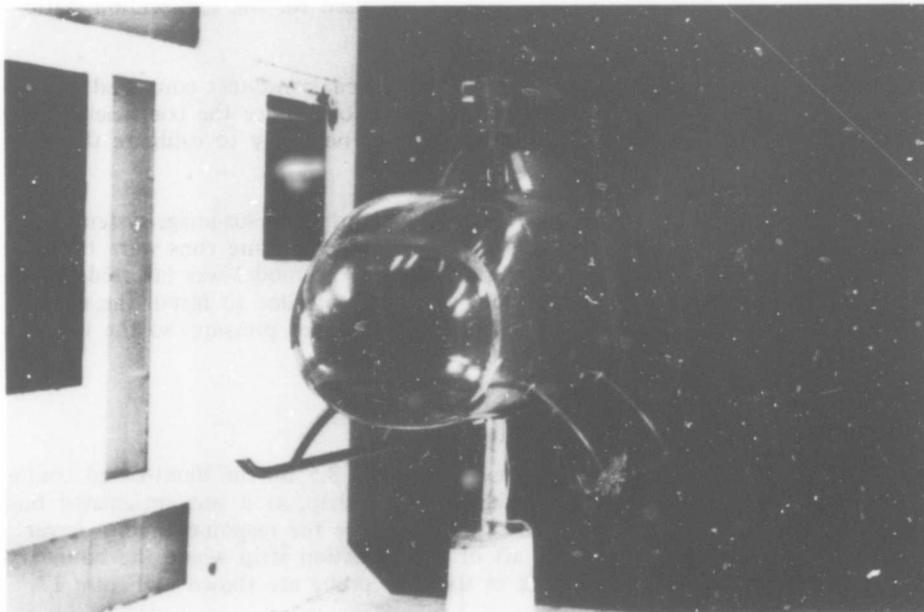
Figure 15.   BO-105 Fuselage Model Mounted in Wind Tunnel.
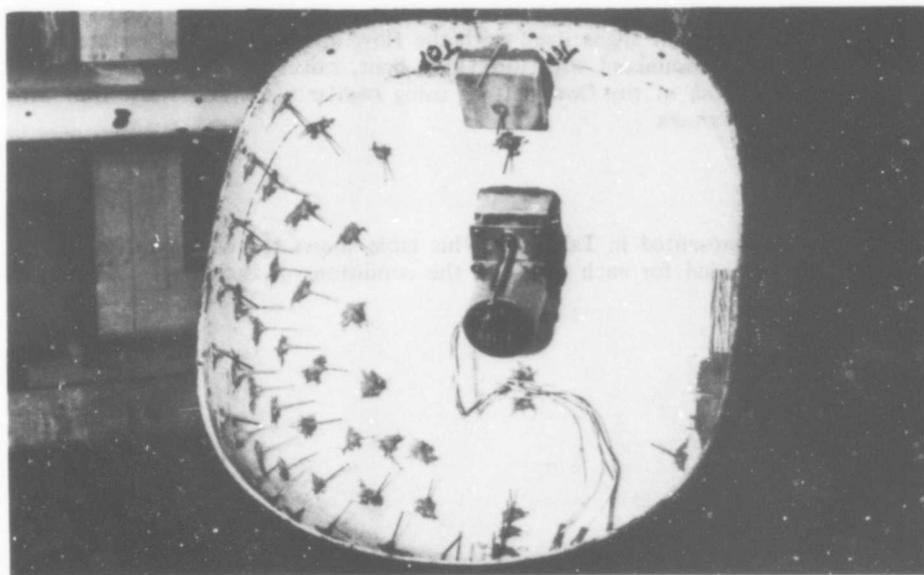
Figure 16.   Boundary Layer Probe Traversing Mechanism
Mounted in Blunt Nose.

44

SOLDER

.032 DIA. STAINLESS STEEL TUBING

.062 DIA. BRASS TUBING

1.25

.625

.25
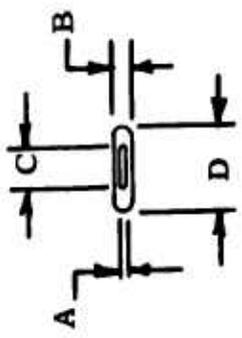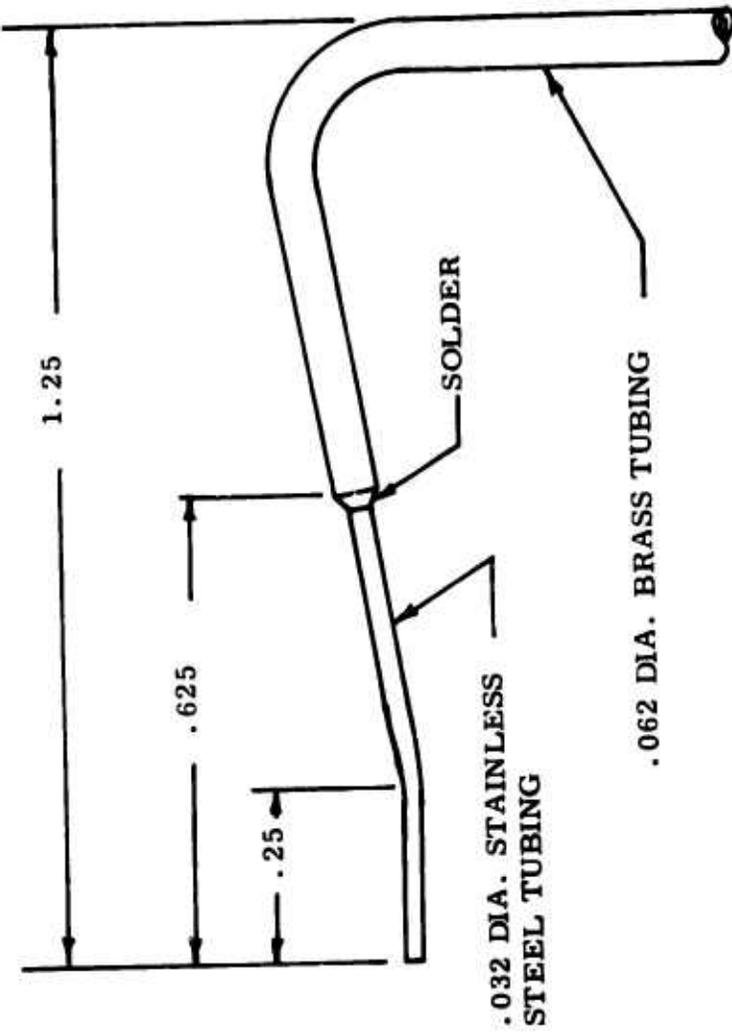
	SMALL PROBE	LARGE PROBE
A	.004	.010
B	.012	.019
C	.028	.027
D	.040	.039

Figure 17. Boundary Layer Probes.

TABLE I.	LOCATION OF PRESSURE ORIFICES IN BASIC FUSELAGE									

FUSELAGE STATIONS

Top ℄	Waterline 14	12	10	8	6	4	2	Bottom ℄	WL 6 Opp Side	Tail Boom Max Width
13	13	13	13	13	13	13	13	13	13	.
15	15	15	15	15	15	15	15	15	.	.
17	17	17	17	17	17	17	17	17	.	.
19*	19	19	19	19	19	19	19	19	19	.
21*	.	.	.	.	.	.	.	21	.	.
23*	.	.	.	.	.	.	.	.	.	.
25*	25	25	25	25	25	25	25	.	25	.
27*	.	.	.	.	.	.	.	.	.	.
29*	29	29	29	29	29	29	29	.	.	.
31*	.	.	.	.	.	.	.	31	.	.
33*	33	33	33	33	33	33	33	33	33	.
35*	35	35	35	35	35	35	35	35	.	.
37*	37	37	37	37	37	37	.	37	37	.
39	39	39	39	39	39	39	.	39	.	.
40.5	40.5	40.5	40.5	40.5	40.5	.	.	40.5	40.5	.
41.4	.	.	.	.	.	.	.	41.4	.	41.4
.	.	.	.	.	.	.	.	42.2	.	.
43	.	.	.	.	.	.	.	43	.	43
46	.	.	.	.	.	.	.	46	.	46
55	.	.	.	.	.	.	.	55	.	55
61	.	.	.	.	.	.	.	61	.	61

*Covered when pylon is installed.

TABLE II. LOCATION OF PRESSURE ORIFICES IN STREAMLINED NOSE

FUSELAGE STATIONS

Top ℄	Waterline							Bottom ℄	WL 6 Opp Side
	14	12	10	8	6	4	2		
-5.17	·	·	·	·	-5.17	·	·	-5.17	·
-4.44	·	·	·	·	-4.44	·	·	-4.44	·
-2.9	·	·	·	-2.9	-2.9	-2.9	·	-2.9	-2.9
- .96	·	·	- .96	- .96	- .96	- .96	·	- .96	·
1	·	·	1	1	1	1	1	1	·
3	·	3	3	3	3	3	3	3	3
5	·	5	5	5	5	5	5	5	·
7	7	7	7	7	7	7	7	7	·
9	9	9	9	9	9	9	9	9	9
11	11	11	11	11	11	11	11	11	·

TABLE III. LOCATION OF PRESSURE ORIFICES IN BLUNT NOSE

FUSELAGE STATIONS

Top ℄	Waterline							Bottom ℄	WL 6 Opp Side
	14	12	10	8	6	4	2		
.37	·	·	·	·	.37	·	·	.37	·
.75	·	·	·	·	.75	.75	·	.75	·
1.5	·	·	·	1.5	1.5	1.5	·	1.5	1.5
3	·	·	3	3	3	3	3	3	·
5	·	5	5	5	5	5	5	5	5
7	7	7	7	7	7	7	7	7	·
9	9	9	9	9	9	9	9	9	9
11	11	11	11	11	11	11	11	11	·

TABLE IV. LOCATION OF PYLON PRESSURE ORIFICES		
FUSELAGE STATIONS		
Top ₵	WL 19	WL 18
19.4	.	.
21	.	.
23	23	.
.	25	.
27	27	.
29	29	.
31	31	.
33	33	.
35	35	.
37.2	.	.
.	.	•

*On ₵ of rear surface of pylon.

TABLE V. TEST PROGRAM

Run	Model Configuration					Position		V (mph)	α (deg)	ψ (deg)	Force Data	Remarks
	Blunt Nose	Pylon	Skids	Rotor Hub	Streamlined Nose	Upright	Inverted					
1	X					X		100,200	0	0	X	Press.
2	X					X		150	0	-15 to +15	X	Press.
3	X					X		150	+5	-5,0,5	X	Press.
4	X					X		150	+10	-5,0,5	X	Press.
5	X					X		150	+15	0	X	Press.
6	X					X		150	-5	-5,0,5	X	Press.
7	X					X		150	-10	-5,0,5	X	Press.
8	X					X		150	-15	0	X	Press.
9	X	X				X		150	-15	0	X	Press.
10	X	X				X		150	-10	-5,0,5	X	Press.
11	X	X				X		150	-5	-5,0,5	X	Press.
12	X	X				X		150	0	-15 to +15	X	Press.
13	X	X				X		100,200	0	0	X	Press.
14	X	X				X		150	+5	-5,0,5	X	Press.
15	X	X				X		150	+10	-5,0,5	X	Press.
16	X	X				X		150	+15	0	X	Press.
17	X	X	X			X		150	+15	0	X	Press.
18	X	X	X			X		100,150,200	0	0	X	Press.
19	X	X	X			X		150	-15	0	X	Press.
20	X	X	X	X		X		150	-15	0	X	Press.
21	X	X	X	X		X		100,150,200	0	0	X	Press.
22	X	X	X	X		X		150	+15	0	X	Press.
23					X	X		150	+15	0	X	Press.
24					X	X		150	+10	-5,0,5	X	Press.

TABLE V - Continued

Run	Model Configuration					Position		V (mph)	α (deg)	ψ (deg)	Force Data	Remarks
	Blunt Nose	Pylon	Skids	Rotor Hub	Stream-lined Nose	Upright	Inverted					
25					X	X		150	+5	-5,0,5	X	Pres.
26					X	X		150	0	-15 to +15	X	Pres.
27					X	X		100,200	0	0	X	Pres.
28					X	X		150	-5	-5,0,5	X	Pres.
29					X	X		150	-10	-5,0,5	X	Pres.
30					X	X		150	-15	0	X	Pres.
31					X		X	100,200	0	0	X	Pres.
32					X		X	150	0	15 to -15	X	Pres.
33					X		X	150	-5	5,0,-5	X	Pres.
34					X		X	150	-10	5,0,-5	X	Pres.
35					X		X	150	-15	0	X	Pres.
36					X		X	150	-15	5,0,-5	X	Pres.
37					X		X	150	+10	5,0,-5	X	Pres.
38					X		X	150	+15	0	X	Pres.
39					X		+I.S.°	100,200	0	0	X	Pres.
40					X		+I.S.	150	0	15 to -15	X	Pres.
41					X		+I.S.	150	-15	0	X	Pres.
42					X		+I.S.	150	-5	5,0,-5	X	Pres.
43					X		+I.S.	150	-10	5,0,-5	X	Pres.
44					X		+I.S.	150	+5	5,0,-5	X	Pres.
45					X		+I.S.	150	+10	5,0,-5	X	Pres.
46					X		+I.S.	150	+15	0	X	Pres.
47	X						+I.S.	150	+15	0	X	Pres.

+I.S. denotes Image Support added.

50

TABLE V - Continued

Run	Model Configuration					Position		V (mph)	α (deg)	ψ (deg)	Force Data	Remarks
	Blunt Nose	Pylon	Skids	Rotor Hub	Stream-lined Nose	Upright	Inverted					
48	X						+I.S.	150	+10	5,0,-5	X	Press.
49	X						+I.S.	150	+5	5,0,-5	X	Press.
50	X						+I.S.	150	0	15 to -15	X	Press.
51	X						+I.S.	100,200	0	0	X	Press.
52	X						+I.S.	150	-5	5,0,-5	X	Press.
53	X						+I.S.	150	-10	5,0,-5	X	Press.
54	X						+I.S.	150	-15	0	X	Press.
55	X						X	150	-15	0	X	Press.
56	X						X	150	-10	5,0,-5	X	Press.
57	X						X	150	-5	5,0,-5	X	Press.
58	X						X	150	0	15 to -15	X	Press.
59	X						X	100,200	0	0	X	Press.
60	X						X	150	+5	5,0,-5	X	Press.
61	X						X	150	+10	5,0,-5	X	Press.
62	X						X	150	+15	0	X	Press.
63	X		X				X	100,150,200	0	0	X	Press.
64	X		X				+I.S.	100,150,200	0	0	X	Press.
65	X					X		150	-15,0,15	0		B.L. 1
66	X	X				X		150	-15,0,15	0		B.L. 1
67	X	X				X		150	-15,0,15	0		B.L. 2
68	X					X		150	-15,0,15	0		B.L. 2
69	X					X		150	-15,0,15	0		B.L. 3
70	X	X				X		150	-15,0,15	0		B.L. 3

B.L. denotes boundary layer probe measurement.

51

TABLE V - Concluded

Run	Model Configuration					Position		V (mph)	α (deg)	ψ (deg)	Force Data	Remarks
	Blunt Nose	Pylon	Skids	Rotor Hub	Stream-lined Nose	Upright	Inverted					
71	X	X				X		150	-15,0,15	0		B.L. 4
72	X					X		150	-15,0,15	0		B.L. 4
73	X					X		150	-15,0,15	0		B.L. 5
74	X	X				X		150	-15,0,15	0		B.L. 5
75	X					X		150	-15,0,15	0		B.L. 6
76	X					X		150	-15,0,15	0		B.L. 7
77	X	X				X		150	-15,0,15	0		B.L. 7
78	X					X		150	-15,0,15	0		B.L. 8
79	X	X				X		150	-15,0,15	0		B.L. 9
80	X	X				X		150	-15,0,15	0		B.L. 9
81	X	X				X		150	-15 to +15	0		Oil
82	X	X				X		100,200	0	0		Oil
83	X					X		150	-15,0,15	0		Oil
84					X	X		150	-15,0,15	0		Oil
85					X	X		100,150,200	0	0		B.L. 9
86					X	X		100,150,200	0	0		B.L. 8
87					X	X		100,150,200	0	0		B.L. 7
88					X	X		100,150,200	0	0		B.L. 6
89					X	X		100,150,200	0	0		B.L. 5
90					X	X		100,150,200	0	0		B.L. 4
91					X	X		100,150,200	0	0		B.L. 3
92					X	X		100,150,200	0	0		B.L. 2
93					X	X		100,150,200	0	0		B.L. 1